University of Alberta

Mechanisms of Aerosol Formation in Bitumen Cracking

by

Pedro Rafael González Delgado 

A thesis submitted to the Faculty of Graduate Studies and Research in partial fulfillment of the requirements for the degree of Master of Science

in

Chemical Engineering

Department of Chemical and Materials Engineering

Edmonton, Alberta
Fall 2004

Your file Votre référence
ISBN: 0-612-95755-1
Our file Notre référence
ISBN: 0-612-95755-1

To Erika

ACKNOWLEDGEMENTS

I would like to thanks Murray Gray for guiding me through out this marvellous learning experience.

To William McCaffrey for his support and advice since I first visit the department two years before I started the program.

To the upgrading group and the support staff of the Chemical and Material Engineering department, specially Tuyet, Leanne, and AnnMarie.

To Oswaldo for his always interesting discussions.

To all the friends and colleagues whose discussions have enriched this project.

To Craig McKnight, Ian Rose, and all the upgrading team of Syncrude Canada Ltd. Research for the encouraging discussions.

And finally I would like to acknowledge the Syncrude and the National Science and Engineering Research Council of Canada Industrial Research Chair in Advanced Upgrading of Bitumen for the financial support of this project.

TABLE OF CONTENTS

LIST OF TABLES

LIST OF FIGURES

LIST OF SYMBOLS

a Parameter in the equation of state

b Parameter in the equation of state

B.P. Boiling Point, °C

D_{vm} Volume median diameter i.e. the diameter corresponding to 50 % in the cumulative volume curve, μm

E_a Activation energy, kJ/mol

$\hat{f}$ Fugacity in a mixture

F Molar flow rate

k kinetic rate constant, s^{-1} or $cm^3/(mol.s)$

K K-value for vapour-liquid equilibrium calculations

k_{ij} Interaction parameter

L/F Liquid fraction in flash calculations

MCR Microcarbon residue, wt%

p Total pressure, kPa

P_c Critical Pressure

P_r Pressure of the reacting mixture, kPa

p_s Equilibrium pressure at the dew point, kPa

P^{sat} Saturation pressure

Q Total volumetric flow

R Ideal gas constant, 8.3145 J/(mol.K)

r Rate of formation, mol/s

S Saturation ratio

T Temperature, °C

T Time, s

T_b Boiling Temperature, °C or K

T_d Dew Point, °C

T_M Initial dew point of the model reacting mixture, °C

T_r Temperature of Reaction, °C or K

V Volume of the reactor

V/F	Vapour fraction in flash calculations
x	Liquid phase molar fraction
Y	Composition of the vapour phase, in molar fraction
y	Vapour phase molar fraction
Z	Compressibility factor
z	Molar fraction of the feed

Greek Letters

$\hat{\phi}$	Fugacity coefficient in a mixture
ρ	Molar density
τ	Space time
ω	Acentric factor

Superscript

f	Value after the reaction, i.e. at $t = t_r$
i	Value before the reaction, i.e. at $t = 0$

Subscript

i	Component i

1. INTRODUCTION

The province of Alberta has enormous resources of bitumen and heavy oil in the form of oil sands. Bitumen and heavy oil must be converted into more valuable commercial products in order to compete with the conventional light sweet crudes. Suncor Ltd., Syncrude Ltd., Husky Bi-Provincial, and recently Shell Canada Scotford Upgrader are facilities that convert the highly viscous bitumen fractions into a synthetic sweet blend. Over 50 % of the residue (petroleum fraction with boiling point +524 °C) converted in North America and Venezuela is processed using coking technologies (Gray, 2003). In Alberta, fluid coking is an important process for which transforming the heaviest fraction from upstream units into distillate products, gases, and the carbonaceous material known as coke, or petroleum coke. In order to increase the efficiency and reduce the cost of fluid coking, and downstream operations, we need to understand the mechanisms that control fouling processes.

This work is aimed at understanding and evaluating the mechanisms of the formation of aerosols in the fluid cokers, in order to assess the impact on downstream equipment fouling and plugging problems. Aerosols, by definition, are solid or liquid particles suspended in a gas medium. Aerosols are known to lead to problems in plant operation like incomplete separation and transport of undesirable material into downstream stages, among others. In the context of upgrading operations aerosols may contribute to carry-over of heavy material and mineral

solids, thus causing fouling and plugging in downstream equipment as process filters and hydrotreaters.

In fluid coking the high-boiling components of bitumen or petroleum are cracked to give vapour. As the vapour passes out of the reactor, it cracks further to give a lower molecular weight product. In the liquid phase, polymerization reactions are more favourable and a substantial amount of coke is formed. The high density of the liquid phase favours recombination and polymerization much more than the vapour phase. Consequently, formation of aerosol droplets in the fluid cokers by heterogeneous condensation, nucleated by the dusty environment, could lead to the formation of polymerized, adhesive material that would affect fouling in the coker and in downstream process units. Chapter 2 presents the background literature on aerosol formation and trapping, and the implications on the fluid coking process.

From the several mechanisms that can lead to heterogeneous condensation the following hypothesis was studied:

1.1. RESEARCH HYPOTHESIS

Heterogeneous condensation due to gas phase chemical reactions is an important mechanism for aerosol formation in the fluid coker.

1.2. OBJECTIVES

The objectives of this work are:

- Develop a methodology that can allow the evaluation of the aerosol

formation in upgrading operations due to gas phase chemical reactions.

- Examine the conditions of the commercial operations in light of the results obtained from this methodology.

With these objectives in mind, Chapter 2 also reviews the fluid coker vapour phase composition, gives the basis for the kinetics of the vapour phase reactions, and presents the vapour-liquid equilibrium concepts for dew point calculations.

Due to the complex reactive mixture present in the gas phase of the commercial operation, an indirect approach is proposed in Chapter 3 for determining the likehood of aerosol formation driven by chemical reaction. The detailed methodology is then presented in Chapter 4. The behaviour of simple model compounds at the operating conditions can be predicted if the kinetic and thermodynamic data are available. We assume that the change in the dew point of mixtures of representative model compounds can be used to predict the tendency to form aerosol in the actual coker mixture.

Chapter 5 uses this calculation methodology to examine the effect of the different operating variables on the formation of aerosol, then compares these results with the conditions within the commercial operation. Finally, we present the conclusions and recommendations for future work, to explore and better understand the aerosol formation phenomenon in upgrading operations.

2. LITERATURE REVIEW

2.1. BITUMEN UPGRADING

Alberta's bitumen resources come from surface mineable Athabasca oil sands and in situ production from Cold Lake and Peace River. These deposits are located in the north of the province. Bitumen is characterized by a density over 1,000 kg/m^3 (^{o}API < 10) and a high viscosity over 10^5 mPa.s at 15 ^{o}C. These properties make the transportation of bitumen an extremely difficult task.

The bitumen is currently upgraded by Suncor and Syncrude Ltd. in Fort McMurray, Husky Bi-Provincial in Lloydminster, and the recently inaugurated Shell Canada Scotford Upgrader located near Fort Saskatchewan. In the following sections, the Syncrude Canada upgrading process is described, and to start, Figure 2.1 presents a schematic representation of the process.

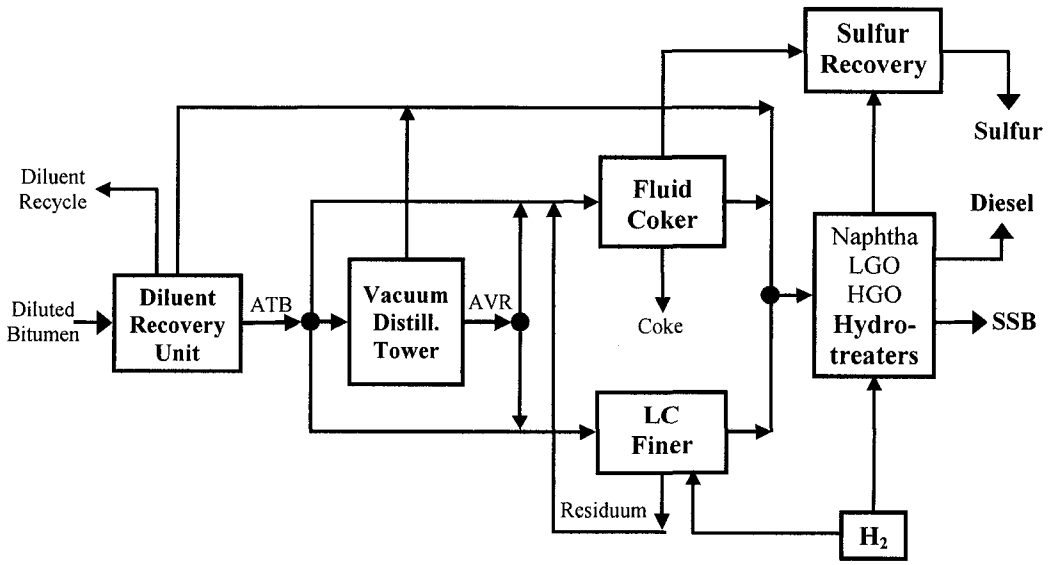

Figure 2.1. Flow diagram of Syncrude process

The Upgrading Plant of Syncrude Canada receives the bitumen diluted in naphtha (boiling point <177 °C) from the froth treatment unit. Naphtha is recovered and returned to the extraction process in the two Diluent Recovery Units. The Diluent recovery units are basically atmospheric distillation units that not only "recover the diluent" but also distill off light gas oil (LGO, B.P. 177-343 °C) and send it directly to a LGO hydrotreater, and from the bottom produce Atmospheric Topped Bitumen (ATB) is obtained, which is then fed to the Vacuum Distillation Tower, LC-Finer, and fluid cokers.

The vacuum distillation tower is a distillation unit operating under vacuum conditions. It distils off light and heavy gas oils (HGO, B.P. 343-524 °C) which are sent directly to hydrotreaters. The residuum from the vacuum distillation tower, known as Athabasca Vacuum Residue (AVR in Figure 2.1), is blended with the remaining atmospheric topped bitumen and sent to the LC-Finer and fluid cokers for further processing.

The LC-Finer is a hydroconversion unit for moderate conversion. It breaks down bitumen feed through cracking and reacting with hydrogen at high pressures (10-15 MPa) over an ebullated catalyst bed. The process produces mainly LGO, however, naphtha, HGO, and light ends are also produced. Naphtha and gas oils are sent to the hydrotreating facilities. Unconverted residuum (B.P. 524 °C+) from the LC-Finer fractionator is sent to the fluid cokers for further cracking.

Atmospheric topped bitumen, vacuum residue, and residuum from the LC-Finer are thermally cracked at low pressure in the fluid coking process, generating

naphtha and gas oil that are sent to hydrotreating, and also coke, sour fuel gas, and flue gas from the burner. The energy required to achieve the endothermic reaction is provided by burning part of the coke.

The final step in the bitumen upgrading is the hydrotreating where hydrogen is added at high pressure in order to reduce the sulfur, nitrogen, and metals content from the product streams and to stabilize the products. The sweet naphtha and gas oils are then blended to produce the Syncrude Sweet Blend.

Plugging and fouling, by clays and heavy materials, reduce the efficiency of the hydrotreating units. This problem is recurrent in the HGO hydrotreater. The main source of heavy material, solids, and minerals in the heavy gas oil hydrotreater may come from the bottom of the fluid coker fractionator. Consequently, in the next section the fluid coking unit and its involvement in the hydrotreater fouling and plugging is discussed.

2.1.1 FLUID COKING UNIT

The combination of the heaviest fractions from the upstream units (diluent recovery, vacuum distillation tower, and LC-Finer) feeds the fluid coker. Table 2.1 shows the properties of the three contributors. The fluid coking units at Syncrude Canada produce approximately 50 % of the feed for the HGO hydrotreating unit. This fraction comes from the bottom of the fluid coker fractionator, thus containing most of the heavy material, fines, and clays entrained from the reactor unit, as will be discussed below. Figure 2.2 shows the schematic representation of the fluid

coker unit.

Table 2.1. Syncrude Canada fluid coker unit feed properties
(Data from Gray, 2003)

Property	Atmospheric Topped Bitumen	Vacuum Residue	LC-Finer Residuum
Contribution, wt%*	38.6	44.8	16.6
API	7	1.6	2.3
Sulfur, wt %	4.8	5.7	2.77
Nitrogen, wt %	0.43	0.58	0.72
Microcarbon residue, wt %	13.6	20.7	21.4
Solids, wt% (Toluene insoluble)	0.24	1.8**	--
Vanadium, wppm	210	319	155
Nickel, wppm	82	125	83
524°C+, vol%	56	87.7	54

*Courtesy of Syncrude Canada Ltd.
**Gray et al. (2003)

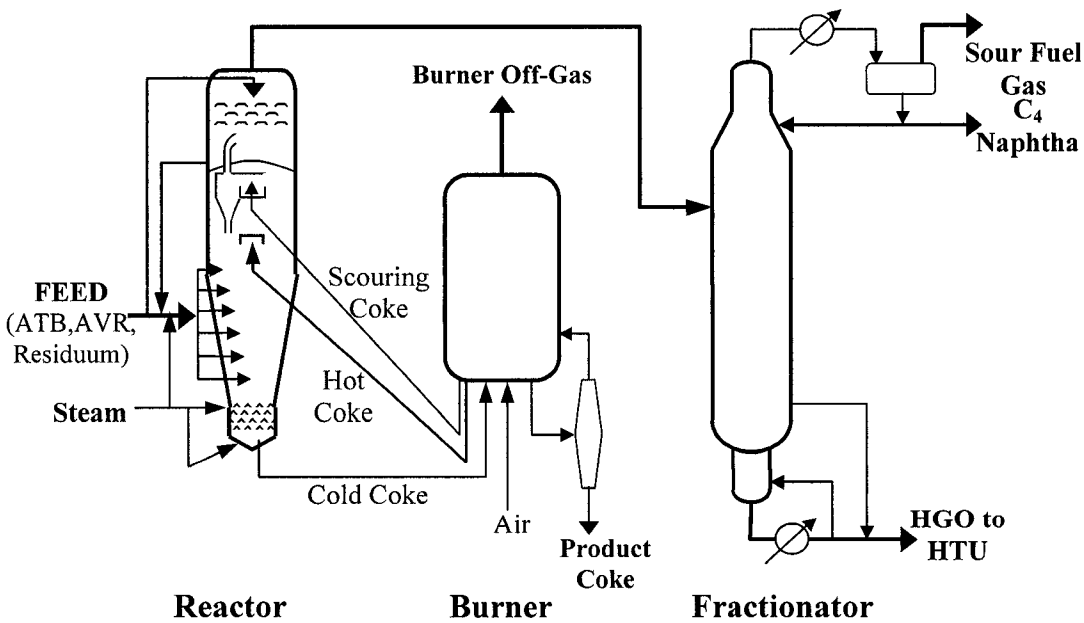

Figure 2.2. Fluid coking unit

The fluid coker feed is preheated to circa 350 °C, then sprayed through two-fluid or pneumatic nozzles into the reactor, using steam as the spraying gas. The mean bitumen droplet size is 300-400 μm, according to estimations by Base et al. (1999). The sprayed feed contacts the fluidized bed, which is made up of hot coke particles coming from the burner with diameters of 100-600 μm. The combined vaporization-reaction of the feed takes place for circa 25 seconds (Gray, 2003) on the surface of the coke particles, which are at temperatures of 510-550 °C, and pressures of 100-350 kPa. The cracked vapour products exit the fluidized bed through a set of cyclones to remove coke particles from the stream. Watkinson et al. (2002) reported a vapour residence time (from surface reaction to cyclone exit) of 6-17 seconds. Afterwards, the vapours are quenched by fresh feed in the scrubbing section of the reactor. This scrubbing section is intended to remove any particles carried in the product vapour. The coke yield on the feed basis, according to Gray (2003) represents 22 wt%, the coke goes to the burner where over 50% of it is burned in order to provide the necessary heat to vaporize part of the feed and for the surface cracking reaction to take place.

The overhead vapour mixture will carry heavy materials, fines, and clays that are not efficiently removed in the cyclones and the scrubber. The mixture then proceeds to be separated in the fractionator, where the heavy material goes to the bottom products, i.e. in the heavy gas oil fraction. Table 2.2 shows the overhead product composition.

Table 2.2. Fluid coker product composition (dry basis)
(Data from Gray, 2003)

Fraction	Composition, wt%
Sour Gas	9.1
Butane	3.6
Naphtha	17.8
LGO*	23.5
HGO*	46.0

*Estimated from Yui (1989).

Carry over of heavy material from the dense bed in the fluid coker reactor might be attributed to the formation of stable aerosol particles. Such particles are able to avoid being removed from the gas stream, so that they will end up in the bottom of fractionator, and ultimately in the hydrotreaters, or they can impinge in the walls of the cyclone producing a coke deposit that can ultimately lead to shut down the fluid coker due to the back pressure. Mallory et al. (2000) and Watkinson et al. (2002) studied recently the cyclone-fouling problem. Mallory et al. (2000) suggested that vapour phase chemical reactions are the cause of fouling. Meanwhile, Watkinson et al. (2002) used closer experimental conditions to the commercial process, indicating that the fouling occur by physical condensation.

In the next section, basic concepts about formation, and removal of aerosols, and their impact on the upgrading process are given.

2.2. AEROSOLS

Aerosol is a very general term given to solid or liquid particles suspended in a gas medium. In this work, the main attention will be given to liquid-particle aerosols, which are also defined as mist and fog. Mists and fogs are suspensions produced mainly by atomization or condensation. The particle or droplet size varies from one author to another. However, Hidy (1984), and Burkholz (1989) defined mists from submicrometer (<1 μm) to about 10 μm. Larger droplets are in the range of sprays.

2.2.1 AEROSOL FORMATION

Two different processes can form aerosols: disintegration and growth or condensation. In this section, three main mechanisms of aerosol formation will be discussed. The first two may be recognized as disintegration processes, forming aerosol by atomization and atomizers, and by entrainment. The third mechanism considered is condensation of components from a vapour phase.

2.2.1.1 Disintegration Processes

ATOMIZATION

The mechanisms for atomization or liquid break-up into droplets are described as follows:

- Droplets in a field of high turbulence: this is the dominant mechanism in distillation trays in the spray regime at high gas velocity, and two-fluid

atomizers, which is the kind of atomizer used in fluid cokers (Base et al. 1999).

- Breakup of a low velocity liquid column: this is the mechanism that governs special applications like prilling towers, widely used in the production of urea.
- Liquid-sheet breakup: a thin sheet that breaks to form what is called "ligaments", which can lead to droplet break-up and formation of finer droplets. This is the basic principle of hydraulic atomizers.
- Single-droplet breakup at very high velocity: this governs the droplet size in free fall and/or sudden acceleration as well as droplet break-up via impingement.

Pressure nozzle, two-fluid nozzles, and rotary devices are the three basic categories of atomizers. In fluid cokers, pneumatic atomizers are preferred using steam as spraying gas.

Base et al. (1999) tested two-fluid nozzles using water and steam as the feed to evaluate designs for fluid cokers, and observed an average diameter of the atomized liquid droplets is in the order of 400 μm. Meanwhile, their proposed improved nozzle is capable of reducing most of the liquid into 300 μm particles (Sauter average mean diameter) from a water-air feed mixture. The Sauter diameter usually corresponds to 70 to 90 % of the volume median diameter (D_{vm}), i.e. the diameter corresponding to 50 % in the cumulative volume graph. The patent does

not show any particle size distribution chart; thus minimum size range could not be found. However, from the Sauter diameter and the cumulative curve for entrainment shown in Figure 2.5, and considering the extreme case the minimum particle diameter is circa 10 μm.

ENTRAINMENT OF LIQUID BY BUBBLE BURSTING

Entrainment of liquid due to gas bubbling and/or jetting through a liquid also forms aerosol. Entrainment is a concern in distillation units as well as in vaporizers and evaporators. In the former case a maximum of 10 wt% of entrainment is permitted before it starts to affect the tray efficiency (Wankat, 1988).

Several different mechanisms can give entrainment of liquid, but the most significant for aerosol formation is bubble bursting. Bursting of bubbles involves two independent physical processes. A bubble going through a liquid eventually reaches the surface forming a thin, dome-shaped film, causing also an oval shallow depression in the liquid surface. The formation of the bubble film is accompanied by a rapid liquid drainage from the top of the dome causing the thinning in this area (if any bubble-stabilizing agent is present it can slow the drainage generating stable foam). It eventually results in the rupture in the apex of the bubble film. The gas trapped inside the bubble at a higher-pressure leaves the bubble rapidly; this helps to break up the bubble film, generating what are called *film droplets* (see Figure 2.3).

A jet of liquid is produced during the bubble film rupture, due to the vacuum effect over the liquid surface at the bottom of the bubble crater. The jet

rises above the liquid surface and "disintegrates" partially into droplets, or *jet droplets* (see Figure 2.3), before it goes back to the liquid. This process is relevant for small bubbles. Once large bubbles or foams are formed over the liquid surface, the generation of jet droplets decreases sharply (Perry et al., 1999, Tomaides and Whitbey, 1976).

Film Droplets Jet droplets

Figure 2.3. Droplets from bubble bursting

In a representative study, Tomaides and Whitby (1976) carried out experiments on bursting of single air bubbles in 0.1 % sodium chloride aqueous solution at two bubble sizes (1.4 mm and 5.5 mm). For 1.4 mm bubbles, the presence of both film droplets and jet droplets was confirmed, while for 5.5 mm bubbles, no jet droplets were observed. The film droplets size observed in both cases were below 50 μm (see Figure 2.4). On the other hand, the jet droplets from the smallest bubble size were above 100 μm in diameter. Consequently, bursting of small bubbles will give the highest yields of aerosol droplets.

Another source of entrainment in contacting equipment occurs when operating at high vapour loads. In this case, the kinetic energy of the vapour is turned into a spray, where larger droplets are formed (>200 μm). In distillation

trays, this mechanism limits the capacity of the tower, since higher levels of entrainment result.

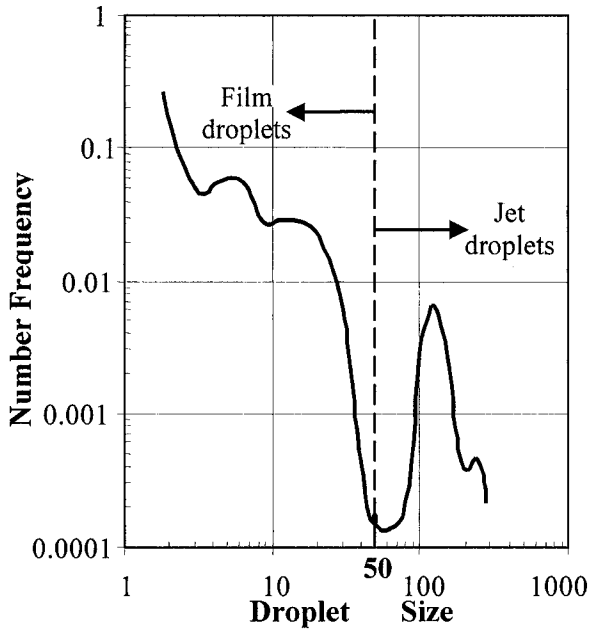

Figure 2.4. Particle size distribution of droplets generated by bursting of 1.4 mm bubbles on a 0.1% NaCl solution
Source: Tomaides and Whitbey (1976).

Typical entrainment droplet size distribution taken from Perry et al. (1999) is shown in Figure 2.5. The log-probability plot presents diameter of particles smaller than 300 μm, due to the fact that the superficial gas velocity at which these data were obtained was 1.3 m/s, which correspond to the terminal settling velocity for a 310 μm droplet for air-water systems (Calvert et al., 1975). In addition, the disengaging space was sufficient to settle out the larger droplets. Less than 10 % of the entrainment was in droplets of less than 50 μm and they were relatively easy to eliminate. However, 50 % of the drops (in number) were under 5 μm. Although this fraction is small on mass basis, these small droplets can serve as a nuclei for

condensation downstream of the equipment, and carry non-volatile material into downstream operations.

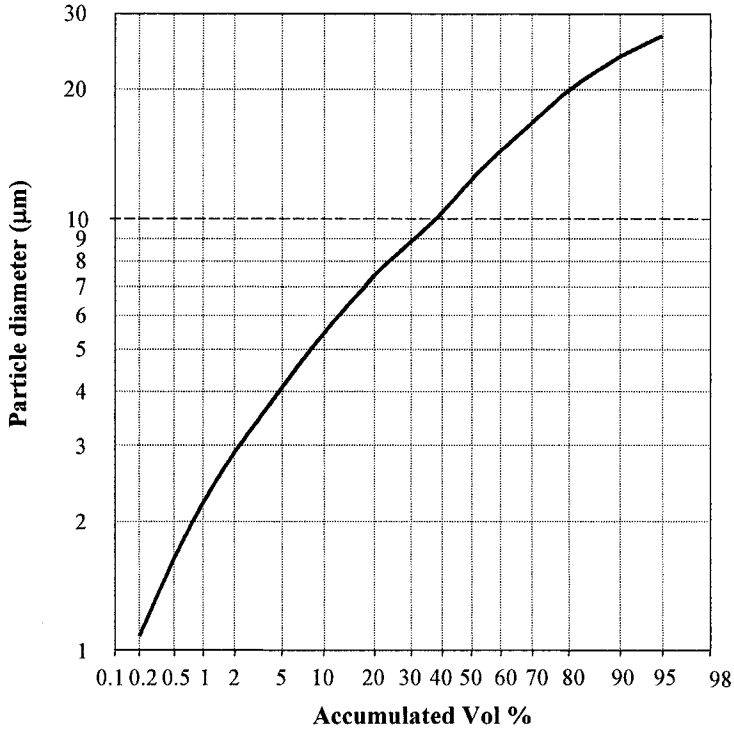

Figure 2.5. Entrainment droplet size distribution for an evaporator with 0.6 m of disengaging space
Source: Perry et al. (1999).

2.2.1.2 Condensation

The formation and growth of liquid aerosol particles by condensation represents a major mass-transfer process between the gas phase and the droplet phase. A necessary condition for this to occur is that the system has to be brought into a state of supersaturation. Saturation in a multicomponent mixture of an inert carrier gas phase and N condensable components can be defined as:

$$S = \frac{p(T, y_1..y_N)}{p_s(T, y_1..y_N)} \tag{2.1}$$

where p is the actual total of all the vapour components (including the inert gas) and p_s the total equilibrium pressure at the dew point of the vapour mixture.

Supersaturation ($S > 1$) can appear if the dew point line is crossed by the process path, which describes the change of state of the gas phase. Mixing of two saturated streams at different temperatures, isentropic or adiabatic expansion of the gas, cooling of the gas by a cold stream, or a cold spot are only some of the many processes based on simultaneous mass and heat transfer that would lead to supersaturation.

Another mechanism for achieving supersaturation is chemical reactions that produce condensable components.

NUCLEATION

The saturation (S) has to exceed a critical barrier before nucleation followed by aerosol formation can take place. Two different mechanisms of nucleation are widely known:

Homogeneous Nucleation

When the nuclei or critical molecule cluster are formed only by condensable components alone, the nucleation is homogeneous. This mechanism requires high supersaturation values ($S > 2\text{-}5$), and is mainly attributed to the Kelvin effect which considers the energy barrier (surface tension) to be overcome in order to create the critical nuclei.

Heterogeneous Nucleation

If gas-borne particles are present, aerosol formation can be initiated by heterogeneous nucleation, which requires very small critical supersaturation even with an insoluble foreign particle, as long as it has been wetted by the liquid. This can easily be the case in a fluid coker, where a dusty environment with submicrometer solid particles, mainly from abrasion of coke in the fluid bed and in the burner, and fines from the feed. These particles serve as nuclei for mist formation. Small particle from entrained liquid in the case of distillation units can also serve as nuclei for aerosol formation in downstream equipment.

After nucleation, the aerosol particles grow very rapidly by condensation until the supersaturation of the gas phase disappears. The particle size obtained by condensation is usually in the range of 0.1 μm to 30 μm (Perry et al., 1999). Such wet particles would carry heavy components into distillate products, and could contribute to fouling of downstream equipment.

2.2.2 AEROSOL REMOVAL

Several mechanisms are involved in separating particles from gases: Brownian diffusion, inertial deposition, flow-line interception, gravity settling, electrostatic deposition, and thermal precipitation. The last two mechanisms may be significant in electrostatic collectors and non-isothermal processes, respectively. Such cases fall out of the scope of this work. Brownian diffusion and inertial deposition are present in most of the collecting devices. Figure 2.6 shows these two

mechanisms in action.

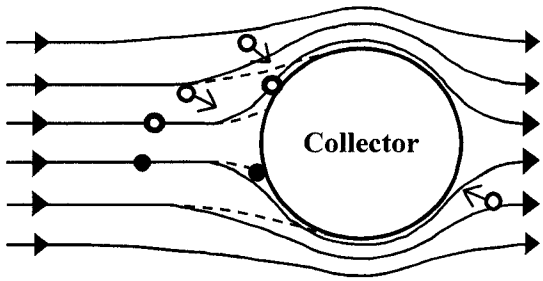

Figure 2.6. Mechanisms of particle collection
Particle collected by: • Inertial deposition. o Streamline deposition.
♂ Brownian Diffusion

Inertial deposition is often the controlling mechanism for removal of particles with diameters over 1 μm in filters, scrubbers, cyclone separators, and other impingement separators like wire mesh, packed bed and baffles. Its principle is based on the deposition of droplets that deviate from the gas streamline when approaching a collecting body due to their inertia, so that the droplets can strike the collector. Along with inertial deposition, there is flow-line interception, when a droplet can be separated from the gas by contact with the collector while following a gas streamline that passes very close to the collector. According to Burkholz (1989), the inertial impaction collection efficiency is affected by two factors. First, the velocity distribution of the gas flowing by the collector, which depends on the Reynolds number of the gas with respect to the collector, and second the drop trajectory, which varies with the mass and air resistance of the drop, and the size and shape of the collector.

Smaller particles (under 1 μm) are subjected to Brownian movement, i.e. particles move randomly, then diffusing from the gas to the surface of the collector.

Different from inertial deposition, the collection efficiency by Brownian diffusion increases with decreasing droplet size and the gas velocity. The so-called diffusional separators do not present Brownian diffusion as the only collection mechanism but also inertial impaction. The influence of these two mechanisms in the collection efficiency, and the effect of the drop size and the gas velocity are schematically shown in Figure 2.7. A remarkable characteristic of this type of equipment is the high operating pressure drops.

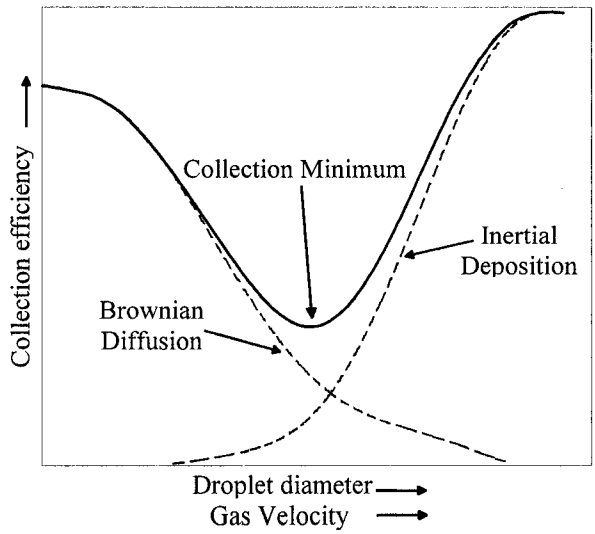

Figure 2.7. Schematic representation of the collection efficiency for a typical diffusional separator

In the following section, cyclone separator and wet scrubbers will be discussed as aerosol collection equipment.

2.2.3 Collection Equipment

2.2.3.1 Cyclone Separator

Cyclones are the most widely used type of solid particle collection equipment, in which the particle rich stream enters tangentially to a cylindrical or conical chamber, where due to the centrifugal force of the order of 5 to 2500 times gravity, particles tend to move toward the outside chamber wall by inertial impaction and removed by gravity settling, while the gas leaves through a central opening. According to Coker (1993), Burkholz (1989), and Perry et al. (1999), these units are limited by a low efficiency for collection of particles smaller than 5 μm. Cyclones can be more efficient on liquid than on solid particles if coalescence and easy drainage are taken into account in the design, also the prevention of re-entrainment has to be considered. The cyclones located in the fluid coker were designed to remove coke particles in the order of 150 μm, hence, easily allowing smaller particles to continue to the subsequent stages.

2.2.3.2 Wet Scrubbers

Scrubbers are units that employ a liquid to help in the removal of particles from gas. Scrubbers can take many forms and are mainly used in solid particle collection, presumably because they are more complex and expensive than impaction devices. Perry et al. (1973) provide a good selection guide, showing the minimum particle size collectible in different types of scrubbers (Table 2.3).

Schifftner and Hesketh (1983) indicate that spray scrubbers efficiently remove 90 % of particles greater than 5 μm, while for cyclone spray, and impingement scrubbers the typical efficiency for > 5 μm particles is 95 %.

Recently, Schaber and coworkers (1995, 2002) studied the formation of aerosol for HCl-water systems in gas-liquid contact devices for wet scrubbing and absorption processes. They affirm that these processes generate aerosols by heterogeneous condensation with mean particle diameters in the range of 1 to 3 μm, when foreign nuclei are present.

Table 2.3. Minimum particle size for various types of scrubbers
(Data from Perry's Handbook 5th ed, 1973)

	Pressure drop, in. water	Min. Particle size, μm
Spray towers	0.5-1.5	10
Cyclone spray scrubbers	2-10	2-10
Impingement scrubbers	2-50	1-5
Packed and Fluidized bed scrubbers	2-50	1-10
Orifice scrubbers	5-100	1
Venturi scrubbers	5-100	0.8
Fibrous-bed scrubbers	5-110	0.5

In order to increase the removal of particles of diameter below 5 μm from the scrubbers, "mist eliminators" or entrainment separators are used with efficiencies of the order of 99 to 99.9 % of the liquid droplets (Schifftner and Hesketh 1983, Koch 2002, Perry et al. 1999).

2.3. AEROSOLS IN BITUMEN UPGRADING

Aerosols tend to pass through fluid beds, and are difficult to scrub from gas streams; therefore, aerosol likely contributes to carry-over of heavy material and mineral solids into the coker heavy gas oil. The following is an analysis of the distillation units and the fluid coker, considering the mechanisms for generation and removal of aerosol.

2.3.1 AEROSOL IN DISTILLATION UNITS

Distillation units are used for separating components of a mixture on the basis of differing boiling points. At Syncrude, distillation is used in the diluent recovery unit, the vacuum distillation tower, and the fractionators of the LC-Fining unit and the fluid cokers.

In distillation the main mechanism of aerosol generation is by entrainment. This entrainment, as described in Section 2.2.1.1, produces a range of particles from below 25 μm (from film droplets) to over 200 μm (spraying for high vapour loads). Most of the entrainment can be captured on the underside of the next higher tray. Smaller particles could pass through the tray openings or valves, but significant capture would occur in the liquid on top of the tray. The aerosol material passed at this point would represent a very low level of "contamination" that would eventually be scrubbed out in the subsequent trays. The lack of any significant clay plugging in the naphtha hydrotreaters, even during episodes of severe plugging of the gas oil hydrotreaters in Syncrude's operations, shows that the multiple contact

stages in the coker fractionators are very effective at scrubbing out the aerosols and passing the solids and heavy components into the coker heavy gas oil. This principle can be extended to the other distillation units.

However, not all the heavy material ends up in the bottom of a distillation tower. Some of this material can be entrained into the contiguous fraction cut, e.g. clays in the LGO hydrotreaters comes from the diluent recovery unit, which has as bottom product the atmospheric topped bitumen and the LGO is extracted from the next upper outlet of this unit. Table 2.4 shows for the four distillation units the streams that might contain contaminations from aerosols.

Table 2.4. Aerosol in distillation units

Unit	Diluent recovery	Vacuum	LC Finer fractionator	Fluid coker fractionator
Main Stream for contaminants	ATB	AVR	LC Finer Residuum	CGO
Stream for entrained aerosols	LGO	Vacuum GO	LC Finer GO	CGO

2.3.2 AEROSOLS IN FLUID COKER UNITS

Feed entrainment likely represents a very small contribution to aerosol since the average droplet size of the sprayed feed is around 300 – 400 μm and the dense bed will collect them by inertial impaction on the surface of coke particles where coking occurs. Ghadiri et al. (1993) found very low collection efficiencies during

the filtration of gasifier fines in fluidized beds for particles below 10 μm. These particles escaping from the dense bed will eventually reach the cyclones.

On the other hand, the fluid coker, as mentioned before, represents an extremely dusty environment; where the fines, small coke particles, and heavy material like asphaltenes can serve as condensation nuclei. These particles would condense whenever the vapour components present in the bed are in a supersaturated state, i.e. condensation will occur as soon as the dew point of the vapour mixture is reached. The droplets size will range from 0.1 to 30 mm which make them hard to remove.

The importance of this mist formed by heterogeneous condensation driven by any of the above situations is that once in the liquid phase at high temperatures the addition and polymerization reactions will be favoured. These reactions would crosslink the material, making it less prone to re-evaporate even at higher temperature zones, like the free board. Also, the material can become more adhesive, giving greater fouling potential, e.g. the droplets can easily impregnate in the walls where further dehydrogenation and polymerization can formed coke. In contrast, the aerosol formed in the scrubber would be much cooler, reducing the subsequent addition reactions.

The aerosol escaping from the fluid coker unit will mainly go to the bottom of the fractionator as mention earlier; hence ending up in the hydrotreaters. Clays and metals (nickel and vanadium) are expected to produce plugging in the hydrotreaters. These materials come mainly from the fines and asphaltenes that

were entrained in form of aerosols. The liquid material of the aerosol *per se* would represent a minor effect on the hydrotreating operations.

The following situations could lead to an increase in dew point:

- Mixing of two streams at different temperatures, which can occur by the contact between the scrubbing liquid and the gas stream in the scrubber, by the steam used for fluidization in contact with the gases in the dense bed, and by the injection of liquid bitumen as feed. The quenching of hot gases in the scrubber would almost certainly gives aerosol.
- The presence of cold spots in the unit, such as the vicinity of the feed nozzles as noted above and the cyclone outlet, which is submerged in a pool of scrubbing feed.
- Chemical reactions in the gas phase such as: a) combination reactions such as addition of olefins, b) unimolecular reactions such as ring closure or isomerization that decrease the saturation pressure, or c) hydrogen abstraction reactions to give aromatics with decreased saturation pressures (i.e. higher boiling point).

The first two situations exposed above that can lead to an increase in the dew point would be controlled by heat transfer and the local energy balance, which can be used to get a local saturation value that would indicate the potential for aerosol formation. In contrast, the possible contribution of the chemical reactions mechanisms has not been investigated. Environmental processes giving aerosol by

chemical reactions have been studied intensively due to their contribution to air quality problems, e.g. reaction of ammonia and hydrogen chloride to ammonium chloride in form of fine divided smoke, sulfuric acid production by oxidation of SO_2, the oxidation of NO to NO_2 and then to nitric acid, and organic particulates formed from ozone-olefins reactions (Hidy, 1984, Friedlander, 1977 and 2000). Lately, Pilinis et al. (1987), Pilinis and Seinfeld, (1987), Wexler et al. (1994), Zhang and Wexler (2002), Christensen and Livbjerg (2000), and many others have evaluated computational models to represent this phenomenon. Unfortunately, these studies do not provide insight into chemical condensation in fluid cokers and a literature search has given no references in this area.

Condensation by chemical reactions will involve addition reactions that can form lower vapour pressure components, however cracking and dehydrogenation reactions are present in a high temperature hydrocarbon mixture given smaller components that can dilute the mixture. Hence, a study of the tendency of aerosol formation by chemical reaction has to consider the composition and reactivity of the vapour phase components. Sections 2.4 and 2.5 extend the discussion on the gas phase hydrocarbon mixture composition and reactivity, respectively.

Once supersaturation is reached, particles will grow by condensation to sizes that range from 0.1 to 30 μm. These particles generated by heterogeneous condensation can polymerize at high temperature, becoming stable and cannot be completely removed from the gas stream by the cyclones. Following the cyclones there is the scrubbing section, which is meant to scrub the heavy components in the

gas stream. Impingement with the grids in the scrubber section would give some removal of aerosol, but not complete removal. Furthermore, the efficiency of the grids would decrease as the contact area is reduced with a consequent increase of the local vapour velocity, as in some coker runs when the grids are fouled heavily. The resulting drop in scrubbing efficiency would pass more aerosols into the coker fractionator, and on to the gas oil hydrotreaters. Improvement in the grid design might offer enhanced trapping of aerosols and better resistance to fouling, or at least better performance under fouled conditions.

In conclusion for this section, we propose that aerosols formation due to heterogeneous condensation, whether by chemical reactions or mechanical means, contribute to the carry over of heavy materials and fines, causing severe fouling and plugging in downstream units, e.g. hydrotreaters. In addition, once the liquid droplets are formed they give much more rapid fouling, since they easily impregnate on the equipment walls, and with further dehydrogenation and polymerization can also form coke.

2.4. FLUID COKER VAPOUR PHASE COMPOSITION

The previous sections lead us to consider heterogeneous condensation due to vapour phase chemical reactions in the fluid coker. Continuing with this objective in mind, a better understanding of the vapour phase composition and kinetics are needed.

The feed is sprayed into the fluidized bed, with the liquid bitumen reacting at the surface of the hot coke particles releasing vaporized light feed and cracked vapours. This vapour mixture is a combination of thousands of different hydrocarbon compounds, which cannot be completely analyzed in the reactor. The final product composition shown in Table 2.2 gives the composition in terms of distillation fractions. The table does not include the heaviest fraction, which is washed out in the scrubbing section; this residue fraction represents approximately 17.6 wt% of the total hydrocarbon vapours (Courtesy of Syncrude Canada Ltd.). Table 2.5 shows the available properties for the naphtha, CGO or combined gas oil (mixture of coker LGO and HGO), and residue, and Table 2.6 shows the composition of the sour gas fraction exiting the fluid coker unit.

The bromine number, determined by the ASTM D1159 method, indicates the concentration of olefins present in the mixture. The diene value obtained by titration with maleic anhydride by UOP Method 326-65, gives a measure of the conjugated diolefin content of the sample. The reaction between the maleic anhydride and the conjugated diolefins occurs via Diels-Alder addition. Values are normally only reported for naphtha due to side reactions when these assays are used

for heavier fractions. On a molar basis, therefore, the olefin content is 46.0 mol % and the diolefin content is 4.2 mol % in the naphtha.

Table 2.5. Assay data for fluid coker bed vapour product
(Naphtha data from Yui,1999; CGO data from Yui, 1989; and Residue data Courtesy of Syncrude Canada Ltd.)

	Naphtha	CGO	Residue
Density, kg/m^3	798.4 @ 15°C	980.8 @ 20°C	1000 @ 20°C[A]
Molecular Weight	129	269[H]	598[H]
Sulfur content, wt%	1.44	4.27	-
Nitrogen cont, ppm(wt)	217	2967	-
Bromine Number, g Br_2/100g	57	27*	-
Diene Value, g I_2/100g	8.3	6**	-
Simulated Distillation, °C			
IBP	15	196	291
5%	60	256	392
10%	77	276	438
30%	130	330	516
50%	169	372	560
70%	198	414	607
90%	240	465	731
95%	-	483	-
FBP	290	515	-

[A] Approximate value
[H] Value estimated using HYSYS v3.1
* Bromine number of the HGO fraction taken from Yui and Ng (1995)
** Courtesy of Syncrude Canada Ltd.

Table 2.6. Fluid coker sour gas composition
(Courtesy of Syncrude Canada Ltd.)

Component	wt%
H_2S	6.1
Hydrogen	1.0
Methane	21.4
Ethylene	8.1
Ethane	16.3
Propene	13.3
Propane	12.2
1,3-Butadiene	2.0
Trans-2-Butene	3.1
Cis-2-Butene	3.1
I-Butene	3.1
1-Butene	3.1
i-Butane	1.1
n-Butane	6.1

The light vapour components (sour gas, butanes, and steam) are well known. The naphtha, CGO, and residue do not have specific compounds that can best describe their reactivity. Hence, the best way of classify them is in term of structural groups, involving paraffins, olefins, naphthenes, alkyl aromatics, hydroaromatics, disulfides, thioethers, etc. Khorasheh (1986) developed a procedure to determine concentrations of carbon groups, i.e., α-carbon, paraffinic carbon, naphthenic carbon, and aromatic carbon, from elemental analysis and ^{1}H NMR and ^{13}C NMR data, and reported a structural composition for CGO.

Gray et al. (1992) based on Khorasheh's procedure to report structural

information from a laboratory batch coking reactor for the naphtha, LGO, HGO, and residue fractions. The information includes aromatic, aliphatic, and heteroatomic structures, as well as, total α-carbon, paraffins, naphthenes, and aromatics for each fraction. Gamma methyl carbons were also reported by Gray et al. (1992). They correspond to the methyl carbons bonded at least 3 carbons away from a aromatic or naphthenic ring structure.

From Gray et al. (1992), Khorasheh (1986), Peddy et al. (1992), Yui (1989,1999), and Syncrude information, one can conclude that paraffins, naphthenes, alkyl aromatics, and olefins are the most representative groups in the complex vapour mixture in a fluid coker. This mixture, and hydrocarbons in general, crack spontaneously at temperatures higher than 350 ^{o}C. The following section presents the main thermal reactions of the groups in the gas phase.

2.5. VAPOUR PHASE PYROLYSIS

The conditions under which the vapour-phase reactions occur in the fluid bed coker are:

- Temperature: 510 – 550 ^{o}C.
- Pressure: 100 – 350 kPa.
- Vapour holding time or residence time: 6 – 17 s.

In this section, reactions of paraffins, olefin pyrolysis, along with diolefin additions reactions, naphthenes, and alkyl aromatics are considered for this range of temperature and pressure.

2.5.1 PYROLYSIS OF PARAFFINS

The free radical mechanism governs hydrocarbon pyrolysis. The mechanism involves 3 steps:

1) Initiation by homolytic cleavage of a carbon-carbon bond, introducing the free radical into the reacting mixture.
2) Propagation by radical decomposition, radical isomerization, hydrogen transfer, and radical addition reactions convert reactants into products while keeping a fixed total radical concentration. The most important of these reactions is the radical decomposition, also called β-scission. In this reaction, the carbon-carbon bond β to the radical site breaks, thus forming an α-olefin and a smaller alkyl radical, as shown:

$$R–CH_2–CH_2–\dot{C}H_2 \longrightarrow R–\dot{C}H_2 + CH_2=CH_2 \quad (2.2)$$

or

$$R–CH_2–\dot{C}H–CH_3 \longrightarrow \dot{R} + CH_2=CH–CH_3 \quad (2.3)$$

3) Termination is the combination or disproportionation of radicals to give stable products.

The stability of alkyl radicals depends on the type of C-H bond, primary, secondary, and tertiary; with stability in the order $3^o > 2^o > 1^o$. Reactions typically favour the formation of more stable radicals.

According to Rebick (1983), at low pressure and conversions the main products from pyrolysis of paraffins are α-olefins and small alkane molecules. Also, the reactions are generally first order in reactant.

2.5.2 Olefin Cracking and Addition Reactions

According to Yui (1999) and Yui and Ng (1995) olefin molecules are present in the naphtha and gas oil fractions. Decomposition of olefins, in absence of hydrogen or a catalyst, is similar to paraffins. Addition reactions of olefins with radicals have also been observed at high pressures (Khorasheh and Gray, 1993 a, b, and c).

At low pressure, olefins in presence of diolefins tend to be involved in addition reactions. Sakai et al. (1970) and Nohara and Sakai (1980, 1988, and 1992) proposed the formation and growth of rings due to cycloaddition of

conjugated diolefins (specifically 1,3 butadiene) or allyl radical to olefins. The additions occur via Diels-Alder type reactions. Nohara and Sakai (1992) also concluded that the selectivity for cycloaddition at temperatures between 510 and 590°C in the gas phase is close to 100 %. Figure 2.8 shows typical cycloaddition reactions.

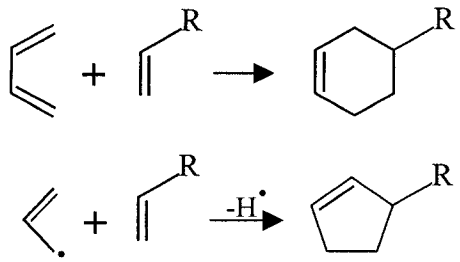

Figure 2.8. Cycloaddition type reactions

Extensive kinetic data have been published by Nohara and Sakai among many others (Kistiakowsky and Ransom, 1939; Rowley and Steiner, 1951; etc.), on cycloaddition reactions between olefins and conjugated diolefins. These reactions are mostly 2nd order reactions in the reactants, i.e. pressure and diluent play an important role in these reactions. Sakai (1983) summarizes most of the kinetic data available, and Nohara and Sakai (1992) extended that work.

The cycloaddition reactions are considered as an early stage mechanism of coke formation under some process conditions. Froment (1990) showed some of the most accepted mechanisms of coke formation from vapour phase components, and they involved unsaturated intermediates. These intermediates can lead to cycloaddition reactions or their addition onto large radicals. The latter mechanism is more probable between a viscous liquid on a surface (large radical) and the gas

phase (olefins). Hence, the former cycloaddition reaction of olefins and diolefins is the most likely mechanism for gas phase reactions under the fluid coker conditions.

2.5.3 Reactions of Naphthenes and Hydroaromatics

Thermal reactions of this group of components are similar to the paraffins, with the addition of ring opening and dehydrogenation reactions. Ring opening and dehydrogenation makes naphthenes less reactive than paraffins (Eq. 2.4). Also, naphthenes and hydroaromatics in absence of hydrogen tend to dehydrogenate to form aromatics (Eq. 2.5) and eventually produce tars and coke. In the case of hydroaromatics, they are considered hydrogen donors, for being able to saturate olefins, and thus hindering the cycloaddition reactions (Eq. 2.6).

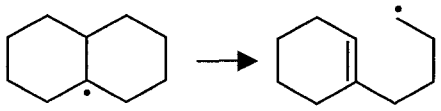

(2.4)

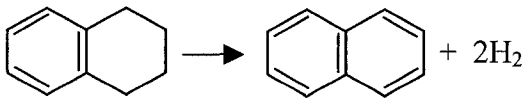

(2.5)

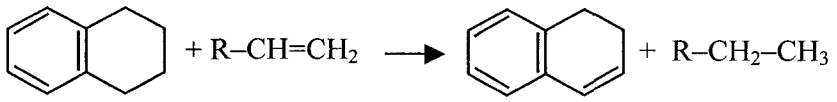

(2.6)

Pyrolysis of the standard hydroaromatic compound 1,2,3,4-tetrahydro naphthalene or tetralin has been studied and kinetic data in the gas phase are available from Mushrush et al. (1988) at 450 °C and Rebick (1980) at 540°C, confirming the high yield of dehydrogenated compounds (1,2- dihydronaphthalene, and naphthalene) at the higher temperature, which is closer to the coker vapour phase temperature.

2.5.4 ALKYL AROMATICS AND AROMATICS

Aromatic rings are very stable at the conditions of interest, and very unlikely to combine and give condensable products. Any reaction of these components will be via side chains.

According to the review by Poutsma (1990), the longer the side chain in alkylbenzenes, the more similar thermal behavior to paraffins they will show. Rebick (1980), and Freund and Olmstead (1989) reported kinetic data for n-butylbenzene pyrolysis at temperatures from 505 to 650 °C in the gas phase, showing that the product distribution involves mainly β-scission of radicals formed at all four carbons of the side chain. The α-carbon was the most suitable for reaction, giving styrene and ethane as main products, as shown.

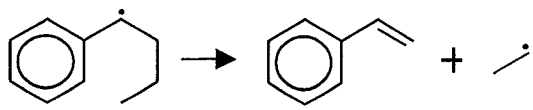

(2.7)

2.5.5 PYROLYSIS OF MIXTURES

In the previous sections, a summary of the thermal behaviour of the main hydrocarbon structural groups in the coker vapour phase was presented. Now the challenge is to put this information together to represent the complex mixture mentioned in Section 2.4. Most of the kinetic and mechanistic information described above involved relatively small molecules, but that information must be generalized to heavier material with boiling points in the range of coker products. Furthermore, in considering pyrolysis of a mixture the free radical reactions are

involved, giving a very complex network of reactions. In an attempt to represent such a complex network, rational simplifications must be considered. Rebick (1983) gives guidelines for such analysis, as follows.

- Compounds with similar cracking mechanisms have little effect on each other.
- More reactive compounds tend to accelerate slower reactants, and vice versa.

At moderate to high severity conditions (high conversions), free radical interactions play an important role in accelerating or inhibiting reactions, as well as changing the selectivity of a certain groups or components (Froment, 1977, 1979; Davis and Williamson, 1979).

2.5.6 Effect of Steam and Hydrogen Sulphide

Steam represents 10 wt% of the vapour mixture, used as spraying gas in the feed nozzles and for fluidization in the lower zone of the reactor. On a molar basis, it corresponds to 47 mol% of the mixture. Steam does not affect the thermal behaviour of hydrocarbons, except for serving as a diluent, thus controlling the partial pressure of hydrocarbons. Nonetheless, a reduction in selectivity to paraffins has been observed in high pressure pyrolysis of hexadecane with excess in steam (Doue and Guiochon, 1969).

Hydrogen sulphide (H_2S) on the other hand, modifies the rate of cracking of hydrocarbons as shown by Rebick (1980) for n-butane, n-hexadecene, 1-dodecene,

n-butylbenzene, and tetralin. H_2S to hydrocarbon partial pressure ratios in these experiments varied up to 1/1 for one particular temperature. H_2S catalyzes the transfer of hydrogen between the reactant and free radicals. In the case of tetralin, the reaction was not accelerated but the selectivity of the products changed drastically, from dehydrogenation to ring opening, when the hydrogen sulphide to tetralin partial pressure ratio was 3/10.

To conclude this section, the main mechanisms in the gas phase of the fluid coker are cracking, by free radicals mechanisms, of the paraffins, alkyl aromatics, and naphthenes. The olefins present in the mixture are likely to produce cycloaddition products in the presence of conjugated diolefins. Dehydrogenation reactions of the naphthenes and hydroaromatics are also an important part of the gas phase reactions. Free radical interactions play an important role at high conversion (high temperature and residence time). Steam, which constitutes 45 mol% of the mixture, does not alter the kinetics of the hydrocarbons at the conditions under study, but the presence of H_2S can affect the rate of the cracking reactions.

2.6. DEW POINT CALCULATIONS

Addition reactions are prone to give condensable products, but, these reactions have to compete against cracking, which diminishes the possibility of formation of aerosols by heterogeneous condensation, as discussed in Section 2.3. The formation of aerosols in the gas phase may cause problems in downstream units. Consequently, we consider the dew point of the mixture during the residence time in the reactor, in order to consider the potential for aerosol formation.

In order to calculate the dew point of any mixture, the components that constitute the mixture and their concentration have to be known at all times. In the case of the fluid coker, the range of components is very diverse, and many of those components have a high molecular weight. For these reasons, the dew point over time for the *real* vapour phase mixture cannot be determined. Nevertheless, model compounds have been used for many years to predict and obtain trends of the real reactive mixtures they intend to emulate. Following the same approach, well-known model compounds that represent the gas phase environment of the fluid coker can be used for estimating the behaviour of the real complex mixture.

2.6.1 VAPOUR-LIQUID-EQUILIBRIUM

A reactive mixture with known constituents can be defined in terms of composition, pressure, and dew point over the reaction time. For calculating the dew point of a mixture, vapour-liquid equilibrium (VLE) calculations are required.

In VLE, the fugacity of a component i in a mixture of n substances in the

vapour phase is equal to its fugacity in the mixture in the liquid phase, i.e.

$$\hat{f}_i^V = \hat{f}_i^L \qquad \text{or} \qquad y_i \hat{\phi}_i^V P = x_i \hat{\phi}_i^L P \tag{2.8}$$

from Eq. 2.8 the *K*-value can be introduced,

$$K_i = \frac{y_i}{x_i} = \frac{\hat{\phi}_i^L}{\hat{\phi}_i^V} \tag{2.9}$$

where P is the pressure, $\hat{\phi}_i^L$ represents the fugacity coefficient of i in a mixture in the phase indicated by the superscript, x, and y represent the composition in the liquid and vapour phase respectively. For dew point determination, given P and y_i, the dew point of the gas mixture is obtained by iterating until the criterion of convergence, shown in Equation 2.10, is fulfilled.

$$\sum_{i=1}^{n} x_i = \sum_{i=1}^{n} \frac{y_i}{K_i} = 1 \tag{2.10}$$

The fugacity coefficients in a mixture depend on the pressure, temperature, and their corresponding phase composition, requiring a double iteration. The simulation package HYSYS v.3.1 of Hyprotech uses a flash calculation, which follows a different treatment of the dew point calculation. First, the convergence criterion is:

$$\sum_{i=1}^{n} x_i - \sum_{i=1}^{n} y_i = 0 \tag{2.11}$$

after the inclusion of Equation 2.8 and a mass balance on a flash drum, Eq. 2.11 can be written as:

$$\sum_{i=1}^{n}\left(\frac{z_i(1-K_i)}{K_i+(L/F)(1-K_i)}\right)=0 \qquad (2.12)$$

here z_i is the composition of component i in the mixture under study. L/F is the liquid fraction, which is set to zero since the vapour fraction at the dew point is one (V/F = 1- L/F). If equation 2.12 is satisfied at a specific T and P, then the mixture is at its dew point.

2.6.2 EQUATIONS OF STATE

In order to obtain the fugacity coefficient we need to define the method of calculation. Equations of state (EOS) are widely used for vapour mixtures. Many different EOS have been developed to date, but the key is in determining the most appropriate one for the nature of the mixture and the set of conditions under which the fugacity coefficients are going to be evaluated. The most common equations of state have a cubic form, e.g. Peng-Robinson (1976) and Soave-Redlich-Kwong (1972). Peng-Robinson (PR) and Soave-Redlich-Kwong (SRK) equations of state are particularly reliable for non-polar substances in general. For gas, oil, and petrochemical applications PR is generally recommended for oil, gas, and petrochemical applications at wide range of temperatures and pressures (> -271°C and < 100 MPa).

The Peng-Robinson EOS can be written as follows:

$$P=\frac{RT\rho}{(1-b\rho)}-\frac{a\rho^2}{1+2b\rho-b^2\rho^2} \quad \text{or} \quad Z=\frac{1}{(1-b\rho)}-\frac{a}{RT}\cdot\frac{\rho}{1+2b\rho-b^2\rho^2} \qquad (2.13)$$

where ρ is the molar density, R the ideal gas constant, and T the temperature. The parameters a and b for pure components are:

$$a = a_c\alpha \quad ; \quad a_c = 0.457235\frac{R^2T_c^2}{P_c} \qquad b = 0.077796\frac{RT_c}{P_c} \tag{2.14}$$

$$\alpha = \left[1+\kappa\left(1-\sqrt{T_r}\right)\right]^2 \qquad \kappa = 0.37464 + 1.54226\omega - 0.26993\omega^2 \tag{2.15}$$

where T_c, P_c, and ω are the critical temperature, pressure, and the acentric factor, respectively. The acentric factor introduced by Pitzer et al. (1955) is defined as,

$$\omega = -1 - \log_{10}\left(\frac{P^{sat}}{Pc}\right)\Bigg|_{T_r=0.7} \tag{2.16}$$

The fugacity coefficient in the vapour phase of a component i in a mixture, which is of our interest for VLE calculation, can be obtained using Equation 2.17.

$$\ln\hat{\varphi}_i^V = \ln\left(\frac{\hat{f}_i^V}{y_iP}\right) = \frac{b_i}{b^V}\left(Z^V-1\right) - \ln\left(Z^V - B^V\right) - \left(\frac{A^V}{2\sqrt{2}B^V}\right)\left(\frac{2}{a^V}\sum_{j=1}^{n}y_ja_{ij} - \frac{b_i}{b}\right)\ln\left[\frac{Z^V+\left(1+\sqrt{2}\right)B^V}{Z^V+\left(1-\sqrt{2}\right)B^V}\right] \tag{2.17}$$

where

$$A^V = \frac{a^VP}{RT} \qquad B^V = \frac{b^VP}{RT} \tag{2.18}$$

The mixture parameters used in Eq. 2.17 and 2.18 are defined by mixing rules,

$$a^V = \sum_{i=1}^{n}\sum_{j=1}^{n}y_iy_ja_{ij} \qquad \text{and} \qquad b^V = \sum_{i=1}^{n}y_ib_i \tag{2.19}$$

and a combining rule is introduced for a^V,

$$a_{ij} = (a_i a_j)^{1/2}(1 - k_{ij}) \tag{2.20}$$

where k_{ij} is known as the binary interaction parameter. The k_{ij} parameter is used to adjust the combining rule to fit the experimental data more closely.

The above equations (2.16 – 2.19) can be also used to determine the fugacity coefficient in the liquid phase. This can be done by changing the vapour phase composition (y) to the liquid phase composition (x), and the compressibility factor (Z^V) to the corresponding Z^L.

As can be seen in the Peng-Robinson EOS, the critical temperature and pressure, the acentric factor, and the binary interaction parameter of the substances need to be known. Data for many relatively small molecules (< 20 carbons) is readily available in the literature and in commercial software packages. When data are not available, there are methods to estimate them. Among these methods, Joback (1984) is considered the best method for the prediction of the normal boiling point (T_b) from the molecular structure with an error of 3.6 % on average. T_b is used in the prediction of many properties. Experimental values are preferred for T_b, since an error will be propagated to other properties calculated with it. Joback (1984) also developed a method to estimate the critical pressure and temperature using as input the structure and the T_b (errors 5 % and 1 % respectively). Riedel (1954) developed a set of equations to determine vapour pressures from T_c, P_c, and T_b (error 2-3 %). The vapour pressure at a relative temperature of 0.7 is used for calculating the acentric factor using Equation 2.16.

Section 2.6 introduced Peng-Robinson EOS for obtaining the fugacity

coefficients. These coefficients are needed to perform the dew point calculations, in order to monitor the formation of aerosols (Section 2.2 and 2.3). This method is valid for a mixture of substances with known physical properties, which is not the case for the vapour phase mixture in the fluid coker (see Section 2.4). However, by selecting model compounds that reflect the composition of the vapour phase in fluid coking and its thermal behaviour, we can determine how the dew point will respond to composition and process variables, and assess the likelihood of aerosol formation. In the next chapter, the development of the procedure followed to determine dew points and estimate aerosol formation is presented.

3. METHODOLOGY

The intention of this work is to evaluate the potential formation of aerosols in the fluid coker due to gas phase chemical reactions. The basis for understanding aerosol behaviour in upgrading operations, the reactivity of gas-phase components, and vapour liquid equilibrium were given in Chapter 2. Here we introduce the approach selected and the methodology, which is developed in detail in Chapter 4.

3.1. MODELING APPROACH

Consider that the fluid coker reactor is held isothermal at a certain temperature (T_r) and isobaric and the vapours from the vaporization-reaction on the surface of coke particles and the feed are present in the vapour phase at a time zero ($t = 0$) at a known composition Y^i, and with a dew point close to T_r. The gas phase mixture starts to react at time $t = 0$ through the different mechanisms described in section 2.5 as it travels from the bed to the outlet cyclones. The reactions will form new compounds, producing changes in the number of moles, which in turn alters the velocity of the vapour phase and ultimately the dew point (T_d) of the mixture.

Ideally, one wants to monitor the gas phase composition and its corresponding dew point variation, and even physically observe if any aerosol is being formed in the process. One would then obtain a profile of the dew point changes of the mixture throughout the reaction time, leading to the hypothetical profiles for different conditions and/or initial compositions of the gas phase

mixture, as portrayed in Figure 3.1. Curve **A** represents a gas phase system in which addition reactions predominate, while curve **B** represents the case where cracking is dominant.

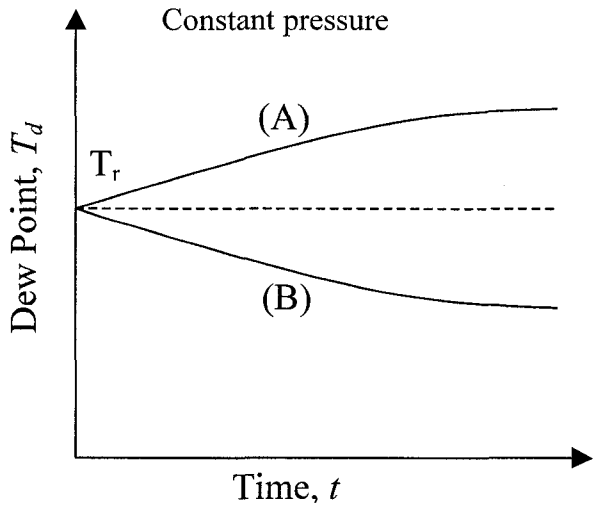

Figure 3.1. Hypothetical dew point profiles

In case (A) aerosol will form as long as nuclei are available, while in case (B) aerosol formation due to chemical reaction is not possible.

In the case of fluid coking, this calculation is complicated by several factors:

- Gas phase is a mixture of thousands of poorly-defined compounds, which cannot be characterized as distinct species.
- Even knowing the composition, the data available for the reaction kinetics of heavy molecules is scarce, and again the network of reactions is extremely complex.

- Equations of state, like PREOS, are very accurate for small compounds, but not in the case of the vapour phase in a fluid coker where the dew point of the mixture is above 500°C. The lack of definition of the components prevents estimations of properties for confidently applying VLE calculations.

These factors rule out simulation of the reactions and phase behaviour for the real mixture. In contrast to the problems associated with the vapour components in a fluid coker, the behaviour of simple model hydrocarbons at 500-550 °C can be predicted from available kinetic and thermodynamic data. These model compounds have dew points well below the reaction temperature, but can be used to determine how dew points will change in response to process conditions and composition. We propose, therefore, an indirect approach to the study of aerosol formation driven by chemical reaction. By selecting model compounds to represent the major reactive hydrocarbon types in the vapour phase in a fluid coker, we can investigate the changes in the dew point of well-characterized mixtures due to reaction. We assume that the change in the dew point of such mixtures will be comparable to the actual reactor material.

Figure 3.2 shows a representation of the dew point profile for the model compounds respect to the real conditions. T_M represents the initial dew point of the model reactive mixture. Again, the curves represent the tendency to form addition products (curve C) or cracking products (curve D).

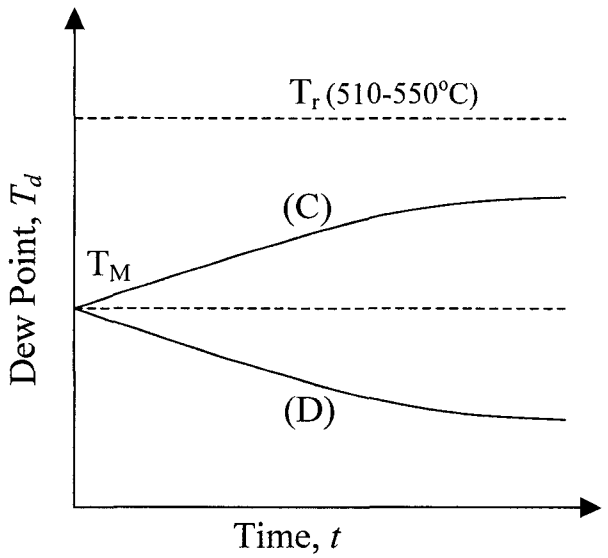

Figure 3.2. Schematic dew point profile for the model mixture

3.2. CALCULATION ALGORITHM

In the following section we present the algorithm for the evaluation of aerosol formation by heterogeneous condensation due to chemical reactions. The approach, based on model compounds is aimed to identify the conditions and compositions where the dew point is constant, based on available known kinetic and thermodynamic data. For this approach we follow the path of calculation shown in Figure 3.3.

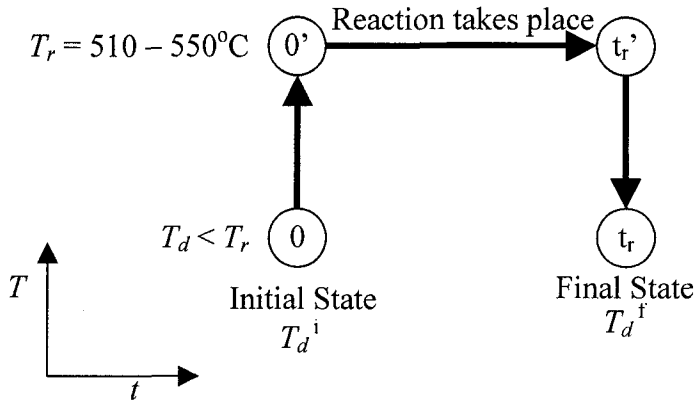

Figure 3.3. Path for calculation of change in dew point due to reaction

The above path shows how the change in dew point due to reaction was determined. The dew point temperature was determined for a mixture of model compounds at the initial state (t = 0). The dew point temperature occurs where saturation pressure (p_s see Equation 2.1) is equal to the total pressure of the mixture. This dew point will be lower than the temperature in the fluid coker for the available model compounds. The mixture of reactants is then considered at state (0'), where the mixture is at the temperature of the coker, and the vapour phase reactions start. The reaction will end at pseudo state (t_r'). At $t = t_r$ the final product

will have a dew point T_d^f which can be compared with the T_d at the initial conditions.

By selecting mixtures of model compounds that contain the same reactive groups as the real mixture in the gas phase, we assume that the change in dew point for the model mixture is the same as the corresponding component types in the fluid coker, that is:

$$\left(T_d^i - T_d^f\right)_{\text{model}} \approx \left(T_d^i - T_d^f\right)_{\text{coker}} \tag{3.1}$$

If the dew point increases with the course of the reaction, as for the model mixture in curve C of Figure 3.2, then aerosol will be expected for the same component types in the coker (Figure 3.1).

Many different sets of operating conditions and initial compositions will lead to aerosol formation and many will not. For a given set of reaction conditions, we are most interested in the boundary between the compositions that favour aerosol formation and the compositions that do not. The search for the boundary will focus on sets of compositions, or regions where the appearance of aerosols will be expected. The general algorithm for finding the boundary is shown in figure 3.4.

Temperature, pressure, and the time of reaction are set, and then inside a loop an initial composition of the model compounds are considered (Y^i). The dew point of that mixture at the pressure specified is obtained through vapour-liquid-equilibrium calculations. The reaction kinetics for the model compounds, using published and validated kinetic data as will be shown in Chapter 4, are used to

calculate the progress of the reaction. The dew point of the final composition (Y^f) is then calculated. The initial and final dew points are compared and if they are different a new initial composition is assumed and steps 3 to 6 of Figure 3.4 are repeated. Once the criterion is fulfilled, the initial conditions (temperature, pressure, and time of reaction) along with the initial composition for the boundary are saved as one limit point. The algorithm was repeated for a range of compositions, thus obtaining a locus of boundary points for a given set of temperature, pressure, and reaction time (T_r, P_r, t_r) that all satisfy the condition $\Delta T_d = 0$.

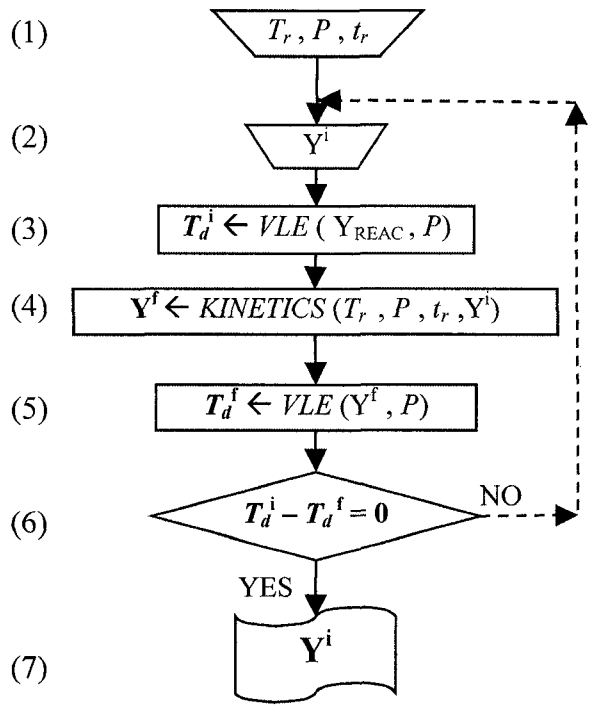

Figure 3.4. General algorithm for searching the boundary for aerosol formation

In order to proceed with the estimation of the boundary limit for the different conditions the following items need to be defined:

- Model compounds to represent the vapour phase at reaction conditions.
- Kinetic parameters of the model compounds.
- Type of the reactor.
- Critical properties of both the model compounds and their reaction products for use in PREOS.
- The parameters and variables of the simulations.
- Presentation of the results.

Next chapter will develop the first four items mentioned above, leaving the last two for the chapter on results and discussion.

4. MODEL DEVELOPMENT

The previous chapter revealed the methodology used to determine the formation of aerosols. Now, this chapter is intended to describe the modeling approach and hence set the basis for Chapter 5 were the results will be presented. Here, the selection of model compounds, their kinetic and thermodynamic properties, the selection of the reactor model, and the software used to generate the results are presented.

4.1. MODEL COMPOUND SELECTION

The criteria for the selection of model compound were the following:

- Compounds shall be a good representation of the real mixture, mainly in terms of their thermal reaction pathways.
- Kinetic information should be available.
- Properties are readily available for VLE calculations, using an equation of state.

From section 2.4, the main structural groups present in the fluid coker outlet were paraffins, naphthenes, alkyl aromatics, olefins, and dienes. Section 2.5 summarizes the main reactions in the vapour phase: cracking reactions of paraffins, alkyl aromatics, olefins, and naphthenes (after ring opening), addition of diolefins to give condensable products, and dehydrogenation of naphthenes and hydroaromatic compounds. These three main reactions will be considered in our

model: cracking, addition of olefins to diolefins, and dehydrogenation.

For this study **n-butylbenzene** (nBB) was selected as a model compound. The alkyl side chain of n-butylbenzene is representative of components in the naphtha, gas oil, and residue fractions which can readily undergo cracking reactions. These gas phase thermal cracking reactions give lower-boiling products, and increase the number of moles to dilute higher-boiling components, relative to longer side change and alkyl bridges, nBB will give a conservative estimate for reaction rate.

The hydroaromatic compound **tetralin** (1,2,3,4-tetrahydronaphthalene) was also used as a model compound, since it dehydrogenates to 1,2-dihydronaphthalene and naphthalene. This component also gives ring opening reactions and subsequent cracking, which is also characteristic of naphthenes as reported by Bredael and Rietvelde (1980) and Hillebrand et al. (1984) for thermal decomposition of cis-decalin and trans-decalin at high temperatures and low pressures. Decalin generally gives light gases and benzene, toluene, and xilene compounds as products. Dehydrogenated compounds, such as naphthalene, have a higher boiling point than hydroaromatic precursors.

Finally, for the addition reaction of olefins and diolefins, **indene** and **1,3-butadiene** were selected. The reactions of 1,3-butadiene have been widely studied, especially by Sakai et al. (1970) and Nohara and Sakai (1980, 1988, 1992). They published data on the gas phase addition reaction of the diene with several different

olefins. Among those olefins was indene, which has a molecular weight and boiling point close to n-butylbenzene. Furthermore, indene has an aromatic ring which is closer to the aromatic materials from bitumen than an α-olefin. The Diels-Alder cycloaddition reaction between these two components leads to the condensation product 1,4,4a,9a-tetrahydrofluorene. The 1,3-butadiene also dimerizes to give vinyl cyclohexene. These addition reactions reduce the number of moles of product and give higher-boiling compounds in the product mixture. These addition reactions also give rise to cyclic products, which are more resistant to subsequent scission than linear addition products. The other type of addition reaction, which can occur, is the termination of free-radical reactions, where two radicals recombine. Due to the low concentration of radicals in the gas phase, these recombination reactions are relatively unfavourable. The products of such reactions were detected but not significant in the kinetic studies of the model compounds selected to represent cracking of bitumen, where data are available, therefore, such termination products are included in the product mixture.

4.2. KINETIC PARAMETERS AND PRODUCT DISTRIBUTION FOR MODEL COMPOUNDS

At the temperature of fluid coking, cracking and dehydrogenation reactions involve a complex set of free radical reactions. Detailed kinetic models to account for these mechanisms have been developed by Froment (1990), and they include the interactions between different components. Given that our approach is to approximate a complex mixture with a highly simplified set of characteristic reactions, detailed mechanistic models were not justified. Instead, we assumed independent reaction of each component. In order to develop a computational program to assess the kinetics of the model compounds we need the order of the reactions, rate constants, and product distribution. This section describes the manipulation of the available kinetic data to adapt it to the requirements of this work.

4.2.1 KINETIC PARAMETERS OF N-BUTYLBENZENE CRACKING

Freund and Olmstead (1989) modeled a pseudo 1^{st} order reaction for the cracking of n-butylbenzene. In the present work, we took into account the experimental data used by the authors for comparison with their model. The experimental data were based on a flow reactor at temperatures 505 – 595°C, and at low n-butylbenzene pressures (40 – 47 kPa). Table 4.1 shows the conversions and reaction times corresponding to three different temperatures.

Table 4.1. Kinetic data for vapour phase cracking of n-butylbenzene
(Data from Freund and Olmstead, 1989)

Temperature, °C	505	536	595
Conversion, %	12.3	8.0	21.9
Space time, s	65.0	12.3	5.5
Product selectivity, %			
Styrene	33.3	32.3	28.6
Ethane	30.3	27.2	20.7
Toluene	8.6	8.6	9.9
Propylene	9.9	9.5	9.8
Ethylbenzene	1.7	1.3	2.2
Ethylene	5.6	8.6	14.4
Allylbenzene	2.6	2.9	2.7
Methane	4.2	5.1	7.8
Propane	0.0	0.0	0.4
Benzene	0.4	0.6	1.1
1,2- Dibenzyl ethane	0.4	0.9	1.1

The experimental first order rate constants were calculated from the experimental data using the plug flow reactor mole balance model, the results are shown in Table 4.2. Afterwards, doing a linear regression on the logarithm of the three rate constants versus the inverse of time makes possible the determination of the pre-exponential and activation energy values for the n-butylbenzene consumption. The pre-exponential factor for nBB cracking is $10^{(10.52 \pm 0.11)}$ and the activation energy (E_a) is equal to 196.3 ± 1.7 kJ/mol.

Table 4.2. Experimental kinetic parameters for n-butylbenzene cracking

Temperature, °C	505	536	595
Exp. first order rate constant, s^{-1}	2.14E-3	7.05E-3	4.99E-2

4.2.2 N-BUTYLBENZENE PRODUCT DISTRIBUTION

Rebick's data reported by Freund and Olmstead (1989) also gave product selectivities for n-butylbenzene pyrolysis. These data were based on a total addition of individual product selectivity of 100 %. This selectivity was used to plot the moles of products versus moles of nBB reacted, as is shown in figures 4.1 and 4.2.

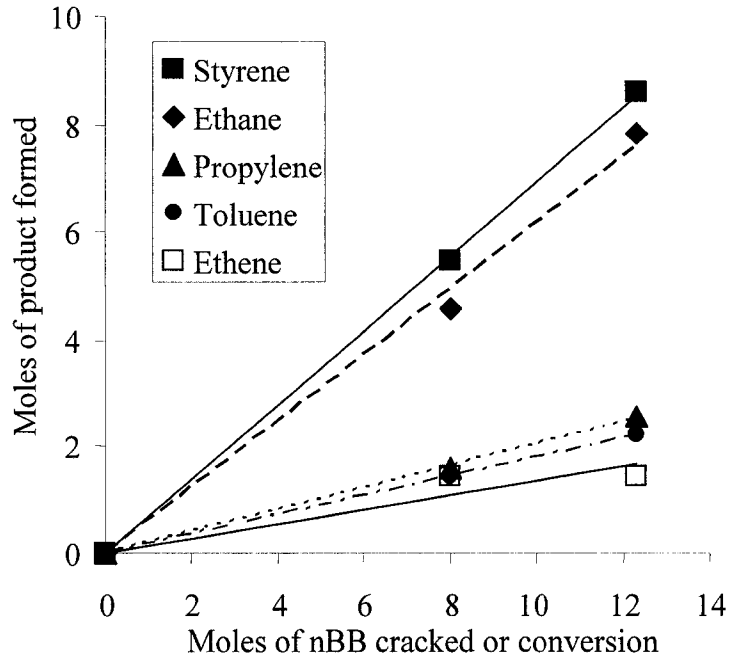

Figure 4.1. Linear regression for nBB products

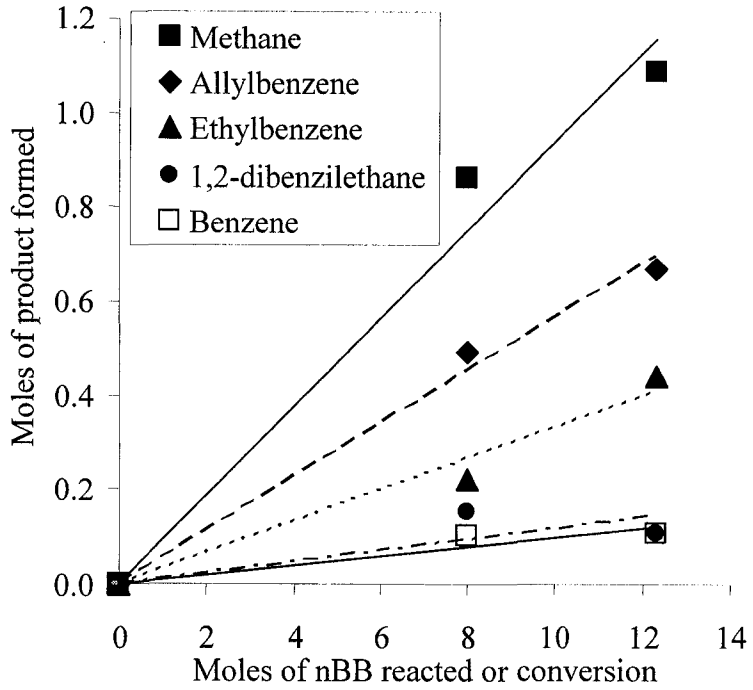

Figure 4.2. Linear regression for stoichiometry of minor nBB products

As shown above, only values reported for 8 and 12.3 % conversion (536 and 505 °C respectively) were used in this analysis, since they are closer to the range under study. Also at 595 °C secondary reactions might change the selectivity. Figures 4.1 and 4.2 show the plots that represent the linear regression for every product of the n-butylbenzene pyrolysis. All products were treated as primary species, to a reasonable approximation, therefore, in determining the coefficients the lines were forced to pass through zero. The slopes of the linear regression are considered the stoichiometric coefficients for the products. These stoichimetric coefficients for a level of confidence of 95 % are listed in Table 4.3.

Table 4.3. Stoichiometric coefficients for n-butylbenzene cracking products (95 % confidence)

Products	Stoichiometric coefficients
Styrene	0.693 ± 0.006
Ethane	0.617 ± 0.020
Toluene	0.1807 ± 0.0003
Propylene	0.206 ± 0.002
Ethylbenzene	0.033 ± 0.003
Ethylene	0.136 ± 0.021
Allylbenzene	0.057 ± 0.002
Methane	0.094 ± 0.006
Benzene	0.010 ± 0.001
1,2- Dibenzyl ethane	0.012 ± 0.003

Appendix C shows the detailed data analysis performed using MS EXCEL for obtaining the slopes. The data from figures 4.1 and 4.2 show that a simplified kinetic scheme, based on a simple decomposition rate is representative for nBB at low conversion.

4.2.3 KINETIC PARAMETERS OF TETRALIN PYROLYSIS

Tetralin pyrolysis has been studied in depth due to its contribution as hydrogen donor in coal processing; therefore, most of this work was carried out in the liquid phase. However, Mushrush et al. (1988) and Rebick (1980) reported

experimental results for pyrolysis of tetralin in the gas phase at 450°C and 540°C respectively.

Mushrush et al.'s (1988) experiments were carried out in constant volume batch reactors, with pressures in the order of 600 kPa, and with times of up to 5 hours. In order to avoid further interferences from secondary reactions only the shortest time was considered here. On the other hand, Rebick's (1980) experiments were held in a more convenient situation since the temperature was within the range of study, the reaction time was short, with lower tetralin pressure, and in a flow reactor. Table 4.4 shows the data from both sources. Since further data were not available, and the main products (from Rebick, 1980) indicate unimolecular reactions, the kinetics of the tetralin thermal reactions were assumed to be first order. Table 4.4 also shows the corresponding first order rate constants. The gas phase thermal cracking of tetralin can be representing by a pre-exponential factor of $10^{11.21}$ and activation energy of 218.6 kJ/mol.

Table 4.4. Kinetic data and parameters for gas phase tetralin thermal reaction
(data from Mushrush,1988 and Rebick, 1980)

Temperature, °C	450	540
Conversion, %	9.0	3.4
Time, s	3600	24
Calculated first order rate constant, s^{-1}	2.62E-5	1.47E-3

4.2.4 PRODUCT DISTRIBUTION FROM TETRALIN PYROLYSIS

According to Poutsma (1990), the reaction of gaseous tetralin at 400-750 °C is characterized by dehydrogenation reactions. Hence, data from Rebick (1980) for product selectivity was used in this work. Table 4.5 shows the reported values. As can be seen in Table 4.5, the information given by Rebick (1980) is incomplete, in that only the larger compounds were given. To correct this, reactions based on the products were balanced as shown in Figure 4.3, and then we calculated the total product distribution or stoichiometry, which is shown in Table 4.6.

Table 4.5. Product selectivity from pyrolysis of tetralin

Product	Selectivity, %
Ethylbenzene and Styrene	4.2
Indene	7.3
C4 Alkylbenzene	4.7
1,2-Dihydronaphthalene	73.1
Naphthalene	10.6

Source: Rebick (1980)

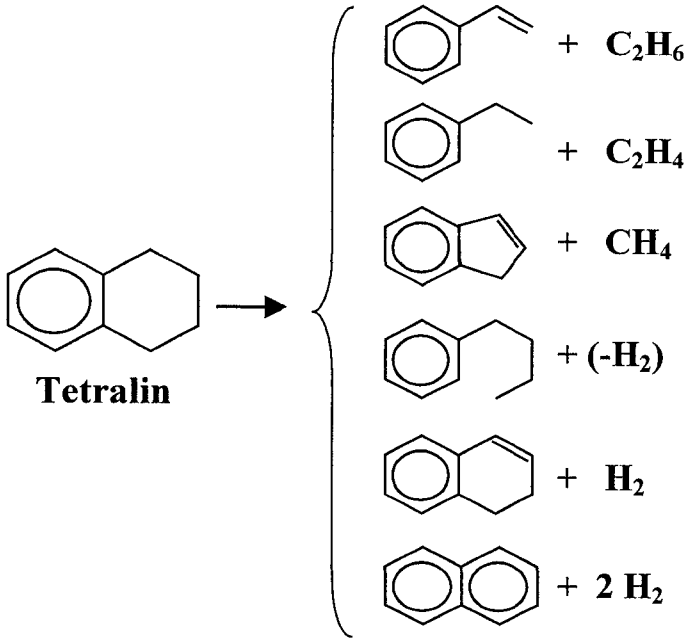

Figure 4.3. Products from vapour phase tetralin thermal reaction

Table 4.6. Stoichiometric coefficients for tetralin pyrolysis products

Products	Stoichiometric coefficients
Styrene	0.021
Ethane	0.021
Ethylbenzene	0.021
Ethylene	0.021
Indene	0.073
Methane	0.073
n-Butylbenzene	0.047
1,2-Dihydronaphthalene	0.731
Naphthalene	0.106
Hydrogen	0.854

Two assumptions were made: 1) Styrene and ethylbenzene selectivities are the same. 2) the C_4 alkylbenzenes are all n-butylbenzene. These assumptions do not add more significant error to the calculations; since the conversion of tetralin and the selectivities in question are relatively small. Furthermore, the boiling points of the corresponding species are close to each other, giving minimal impact on dew point.

4.2.5 Olefin and Diolefin Addition Reactions

The selected compounds were indene and 1,3-butadiene for the olefin and diolefins respectively. Sakai et al. (1970) and Nohara and Sakai (1980, 1988, 1992) studied the addition reaction between these two compounds in the vapour phase. The reactions proceed via a Diels-Alder mechanism as shown in Section 2.5.2. Equations 4.1 and 4.2 show the addition reactions involved between indene and 1,3-butadiene, where first we can see the addition producing 1,4,4a,9a-tetrahydrofluorene (4HF) and second is the dimerization of 1,3-butadiene to form 4-vinylcyclohexene. These additions are second order reactions:

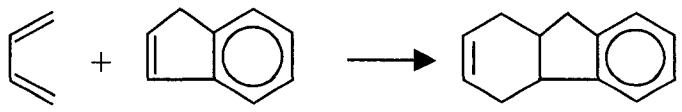

(4.1)

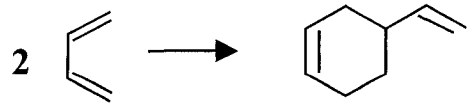

(4.2)

Table 4.7 provides the unpublished values that Nohara and Sakai obtained in their batch reactor experiments corresponding to the equation 4.1 (see Appendix

D). The data were used to obtain the Arrhenius equation as explained before, obtaining a value of R^2 equal to 0.997, giving and pre-exponential factor of $10^{(8.16 \pm 0.22)}$ and an activation energy of 82.8 ± 3.0 kJ/mol.

Table 4.7. Rate constants for the addition of 1,3-butadiene to indene

Temperature, °C	370	390	410	500
Exp. second order rate constant, $cm^3/(mol.s)$	28.1	44.8	61.9	377

The Arrhenius parameters are reliable for giving rate constant values from 370 to 500 °C. However, due the lack of information at higher temperatures, and based on the affirmation by Nohara and Sakai (1992) that the selectivity of cycloaddition is ca. 100 % at temperatures between 510 and 590 °C, this work assumes the Arrhenius parameters to be valid for the range of 510 – 550 °C.

Experimental rate constant values for the dimerization of 1,3-butadiene are given by Sakai et al. (1970) for temperatures in the range of 510 to 590°C. The pre-exponential factor and the activation energy also reported by Sakai et al. (1970) were $10^{(10.41 \pm 0.04)}$ and 103.8 ± 0.5 kJ/mol, respectively.

4.3. KINETIC MODEL

4.3.1 TYPE OF REACTOR

The fluid coker is a continuous flow reactor with a residence time distribution (RTD) that can be represented by a combination of ideal plug flow reactors (PFR) and continuous stirred tank reactor (CSTR). Specific information about the RTD of a fluid coker has not been published; however, Cents et al. (2003) reported that the RTD of the gas phase in a fluidized bed in presence of solids can be represented as 4 to 8 CSTRs in series. In this work both PFR and CSTR models were evaluated, giving some difference in extents of conversion for the model compounds. The boundary for aerosol formation was however, insensible to the type of reactor, as is showed in Appendix B. Given this observation, the model reactor used was the ideal isobaric and isothermal plug flow reactor.

4.3.2 EQUATIONS FOR THE KINETIC MODEL

The governing equation for a PFR is as follows:

$$r_i = \frac{dF_i}{dV} \tag{4.3}$$

where r_i and F_i are the rate of formation and the molar flow rate of component i, respectively, and V the volume of the reactor. Putting together the information from Section 4.2, along with Equation 4.3 we obtain the set of ordinary differential equations (ODE) 4.4 – 4.10 that need to be solved. Note that ideal gas law was used

for substituting the values of the total volumetric flow (Q), and that F represents the total molar flow rate (see Table 4.8 for details on its determination).

$$\frac{dF_{Tet}}{dV} = -k_{Tet}C_{Tet} = -k_{Tet}\frac{F_{Tet}}{Q} = -\left(k_{Tet}\frac{P}{R\cdot T}\right)\left(\frac{F_{Tet}}{F}\right) \tag{4.4}$$

$$\frac{dF_{nBB}}{dV} = -\left(k_{nBB}\frac{P}{R\cdot T}\right)\left(\frac{F_{nBB}}{F}\right) + \left(0.047k_{Tet}\frac{P}{R\cdot T}\right)\left(\frac{F_{Tet}}{F}\right) \tag{4.5}$$

$$\frac{dF_{But}}{dV} = -\left[2k_{Dim}\left(\frac{P}{R\cdot T}\right)^2\right]\left(\frac{F_{But}}{F}\right)^2 - \left[k_{Add}\left(\frac{P}{R\cdot T}\right)^2\right]\left(\frac{F_{But}F_{Ind}}{F^2}\right) \tag{4.6}$$

$$\frac{dF_{Ind}}{dV} = -\left[k_{Add}\left(\frac{P}{R\cdot T}\right)^2\right]\left(\frac{F_{But}F_{Ind}}{F^2}\right) + \left(0.073k_{Tet}\frac{P}{R\cdot T}\right)\left(\frac{F_{Tet}}{F}\right) \tag{4.7}$$

$$\frac{dF_{VCH}}{dV} = \left[k_{Dim}\left(\frac{P}{R\cdot T}\right)^2\right]\left(\frac{F_{But}}{F}\right)^2 \tag{4.8}$$

$$\frac{dF_{4HF}}{dV} = \left[k_{Add}\left(\frac{P}{R\cdot T}\right)^2\right]\left(\frac{F_{But}F_{Ind}}{F^2}\right) \tag{4.9}$$

$$\frac{dF_{C3=}}{dV} = \left(0.206k_{nBB}\frac{P}{R\cdot T}\right)\left(\frac{F_{nBB}}{F}\right) \tag{4.10}$$

In the above equations, P is the partial pressure of the hydrocarbon mixture, T is the reaction temperature, F_{Tet}, F_{nBB}, F_{But}, F_{Ind}, F_{VCH}, F_{4HF}, and $F_{C3=}$ are the molar flows of the 4 model reactants and the molar flow rate of vinylcyclohexene, 1,4,4a,9a-tetrahydrofluorene, and propylene respectively. The two addition products VCH and 4HF are solved by integrating the differential equations since they are

dependant of 1,3-butadiene which is being consumed by both reactions. Meanwhile, since nBB is both consumed by the cracking reaction and generated by the cracking of tetralin, propene was chosen to calculate the net nBB cracked. This number, along with the stoichiometric values showed in tables 4.3 and 4.6 and, was used to calculate the rest of the products of nBB cracking. Table 4.8 summarizes the equations used for calculating the flow rate of the species in the mixture at all times.

MATLAB's built-in function `ode45.m` (Runge-Kutta embedded scheme 4-5) was used for solving simultaneously the non-linear ODEs of initial value type presented above. In order to solve the system of differential equations we need the initial concentration of the reactants (given as variables), the total volume of the reactor, the volumetric flow at the inlet of the reactor (Q_0), and the equation representing F at all times (Table 4.10). Reaction time is one of the input arguments of the modeling approach as shown in Fig. 3.4. In this work we use the space time (τ) defined in eq. 4.11.

$$\tau = \frac{V}{Q_0} \tag{4.11}$$

Once the space time is defined, either V or Q_0 can be selected arbitrarily and the other can be calculated from eq. 4.11. The arbitrarily selection of one of the variables only affect the velocity of the mixture through the reactor but it does not alter the extent of the reactions. Here the total volume was assumed to be 1 m^3 for all the calculations, thus Q_0 could be obtained, and the initial molar flow rate of the

reactants. The concentrations whether in mole fraction or in mol/L, correspond to the initial conditions. The total molar flow rate at any point is simply the sum of all the different species present in the reacting mixture. Table 4.8 shows the total moles from the stoichiometric values for the four reactions involved.

The MATLAB code used for the kinetic model is given in Appendix A.

Table 4.8. Total molar flow rate

	Inlet molar Flowrate	Molar flowrate after reaction
Tetralin (Tet)	F_{Tet0}	F_{Tet} (from eq. 4.4)
n-Butylbenzene (nBB)	F_{nBB0}	F_{nBB} (from eq. 4.5)
1,3-butadiene (But)	F_{But0}	F_{But} (from eq. 4.6)
Indene (Ind)	F_{Ind0}	F_{Ind} (from eq. 4.7)
Vinylcyclohexene (VCH)	0	F_{VCH} (from eq. 4.8)
1,4,4a,9a-Tetra hydrofluorene (4HF)	0	F_{4HF} (from eq. 4.9)
Propylene (C3=)	0	$F_{C3=}$ (from eq. 4.10)
Naphthalene (Nap)	0	$0.106*(F_{Tet0}-F_{Tet})$
1,2-dihydro naphthalene (DHN)	0	$0.731*(F_{Tet0}-F_{Tet})$
Hydrogen (H2)	0	$0.854*(F_{Tet0}-F_{Tet})$
Toluene (Tol)	0	$0.181*(F_{C3=}/0.206)$
Allylbenzene (AB)	0	$0.057*(F_{C3=}/0.206)$
Benzene (Bzn)	0	$0.010*(F_{C3=}/0.206)$
Diphenylethane (DBE)	0	$0.012*(F_{C3=}/0.206)$
Styrene (Sty)	0	$0.021*(F_{Tet0}-F_{Tet}) + 0.693*(F_{C3=}/0.206)$
Ethane (C2)	0	$0.021*(F_{Tet0}-F_{Tet}) + 0.617*(F_{C3=}/0.206)$
Ethylene (C2=)	0	$0.021*(F_{Tet0}-F_{Tet}) + 0.136*(F_{C3=}/0.206)$
Ethylbenzene (EB)	0	$0.021*(F_{Tet0}-F_{Tet}) + 0.033*(F_{C3=}/0.206)$
Methane (C1)	0	$0.073*(F_{Tet0}-F_{Tet}) + 0.094*(F_{C3=}/0.206)$
Total Moles	$F_0 = F_{Tet0} + F_{nBB0} + F_{But0} + F_{Ind0}$	$F = 1.848*F_{Tet0} - 0.848*F_{Tet} + F_{nBB} + F_{But} + F_{Ind} + F_{VCH} + F_{4HF} + 9.898*F_{C3=}$

4.4. THERMODYNAMIC PROPERTIES OF REACTING MIXTURES

In order to execute the VLE calculations with a cubic equation of state, we need reliable critical properties of all the species. With the exception of 1,4,4a,9a-tetrahydrofluorene ($C_{13}H_{14}$), 1,2-dihydronaphthalene, and allylbenzene, all the other compounds critical properties were found in the HYSYS v.3.1 library. Essential information for estimating the critical properties is the boiling temperature, and also, though less relevant, the standard liquid density which happen to be available for 1,2-dihydronaphthalene and allylbenzene from the CRC Handbook (2003). Only 1,4,4a,9a-tetrahydrofluorene did not have any data reported besides its structure and molecular weight, therefore, the method of Joback (1984) was used to determine its normal boiling point. The boiling point calculated was 272 °C. This value is reasonable in comparing with species with similar molecular weight and/or structure, e.g. α-propylnaphthalene ($C_{13}H_{14}$) 274-5 °C, β-isopropylnaphthalene ($C_{13}H_{14}$) 268 °C, 2,3,6-trimethyl naphthalene ($C_{13}H_{14}$) 263-4 °C, and fluorene ($C_{13}H_{10}$) 293-4 °C. Table 4.9 reports the properties and the methods used for their estimation.

Appendix E shows the critical temperature, the critical pressure, the acentric factor and the binary interaction parameters (k_{ij}) for all the compounds used in this work.

Table 4.9. Estimated critical properties

Properties	Method	1,4,4a,9a-Tetra hydrofluorene	1,2-Dihydro naphthalene	Allylbenzene
Normal boiling point, °C	Joback (1984)	272	207*	156*
Critical temperature, °C	Joback (1984)	513	445	368
Critical pressure, kPa	Joback (1984)	2989	3727	3424
Acentric factor	Eq. 2.15**	0.428	0.347	0.319

* Experimental values from CRC Handbook (2003)

** Vapour pressures, used to calculate the acentric factor, were estimated using Riedel's method (1954)

4.5. DETERMINING THE BOUNDARY FOR AEROSOL FORMATION

A full algorithm, given in Fig. A.1 of Appendix A, was developed for the determination of the boundary locus for aerosol formation at a given set of conditions. The algorithm interconnects the three main software packages used:

1. Main Workbook: An MS EXCEL file with different spreadsheets containing all the necessary inputs to run the simulations. It invokes the other two platforms to obtain the solution of the chemical reaction equations and the dew points. Furthermore, it contains its own code (Visual Basic Macros) which execute and coordinate the full algorithm mentioned above to efficiently find the locus of the aerosol formation boundary.
2. Kinetic Program (in MATLAB): Developed in section 4.3, it receives data from the main spreadsheet and returns the concentrations after the reaction.
3. HYSYS V.3.1: The concentration and pressure are the input taken from the main workbook. HYSYS V.3.1 calculates the dew points (initial and final), based on the thermodynamic data discussed in section 4.4, and sends them to the main workbook.

5. RESULTS AND DISCUSSION

In this chapter the results of the simulations of the aerosol formation boundaries are presented for a range of operating conditions. The results are presented in a consistent format of ternary diagrams, to show the aerosol boundary in a two-dimensional composition space. These diagrams were used to analyze the sensitivity of the boundary for aerosol formation to the reacting temperature, pressure, time, presence of steam, and the composition of the reactants. Finally, the boundaries are compared with the available data for the actual coking process and the implications for the fluid coker operations are discussed.

5.1. TERNARY DIAGRAMS

The operating conditions, i.e. reaction temperature, pressure, and reaction time ranges were already defined in Section 2.5, and are summarized in Table 5.1.

Table 5.1. Fluid coker operating conditions

Variable	Range
Reaction temperature, °C	510 – 550
Total pressure, kPa	100 – 350
Reaction time, s	6 – 17
Steam content, wt%	10

For a given initial set of conditions (temperature, pressure, reaction time, steam content, etc) the calculation method developed a locus of compositions to represent the boundary between aerosol and no aerosol formation. For a given initial olefin/diolefin ratio and steam content, each initial composition has two degrees of freedom. With this in mind, ternary diagrams were selected to show the main results of this study. To show the results from the products would be more complicated and less informative since there are 19 components in the model mixture after reaction.

In Section 2.5.6 the steam content was estimated to be 47 mol% (10 wt%) of the total product mixture. This value was set as part of the typical parameters for the calculations. However, for a sensitivity study of the steam content on the boundary for aerosol formation two values for steam content were used: wet (47 mol%) and dry (0 mol%).

In the fluid coker, the liquid feed reacts on the surface of the hot coke particles to evolve the product vapour mixture. The initial vapour-phase composition, therefore, will be a mixture of these evolving components with the local vapour phase in the reactor. These vapours then mix in the reactor and evolve to give the observed product stream. We can estimate the product composition by combining assays from the product streams after fractionation, but we cannot establish the initial vapour composition with confidence. Our approach in this chapter is to consider the sensitivity of the aerosol boundary to the time and extent

of reaction, to determine whether we can use the product composition for calculations.

The initial composition in the vapour phase of olefins and diolefins may depend on several factors, among them, the feed characteristics, the reaction time, temperature, etc. These factors are discussed later in this chapter. To define the olefin to diolefin ratio for the simulations, we used the data corresponding to the olefins and diolefins from tables 2.2, 2.5, and 2.6. This approach assumes that the exit vapour composition can be used to represent the mixture for the purpose of examining aerosol formation. In the vapour phase the olefin content is 27.8 mol% and the diolefin 3.0 mol%. These values include the diolefin and olefin contents of the coker gas oil. The ASTM D 1159–77 and UOP 326–76 test methods can overestimate the olefins and the diolefins concentrations, when applied to fractions heavier than naphtha. If we neglect the bromine number and the diene numbers of the coker gas oil, the results are 15.8 mol% of olefins and 1.1 mol% of diolefins. In this study our objective is to consider the most conservative case, which maximizes the potential for aerosol formation. Hence, the olefin to diolefin ratio used as a typical parameter for the calculations is 9, at the higher end of the two estimates.

The ternary diagrams that will be shown throughout this chapter are on a dry basis, i.e. they illustrate only initial composition of hydrocarbons in the mixture. Each corner of the ternary diagram is associated with the components that represent one of the key reactions of the coker. Cracking reactions of alkyl aromatics are represented by n-butylbenzene (nBB), shown in the left corner. The

dehydrogenation-cracking reactions are represented by tetralin (Tet) in the right corner. The addition reactions of olefin plus diolefin are represented by indene and butadiene (Ind+But) on the peak of the diagram. The olefin to diolefin ratio (O/DO) needs to be fixed for each set of calculations along with steam concentration. Figure 5.1 shows a ternary diagram for the typical fluid coker conditions.

Every point on the boundary line represents an initial composition. On that boundary line the criterion $\Delta T_d = 0$ is satisfied for the specified reaction time and reaction conditions, i.e.:

$$\Delta T_d = \left(T_d^{\mathrm{i}} - T_d^{\mathrm{f}}\right) = 0 \tag{5.1}$$

Each point on the boundary has a different initial and final dew point, because the dew point at the reactor pressure is a function of the vapour composition. Each point will also give a different product composition, but for every point on the boundary the initial and final dew point temperatures are the same.

Figure 5.1 shows that any mixture above the boundary line (region A) will contain more olefin and diolefin content and hence aerosols are expected to be formed in that region. Below the boundary line (region B), cracking reactions will predominate over the addition reactions, therefore, aerosol will not be formed. The following sections examine the position and sensitivity of the boundary line to the initial conditions for the reactor calculations.

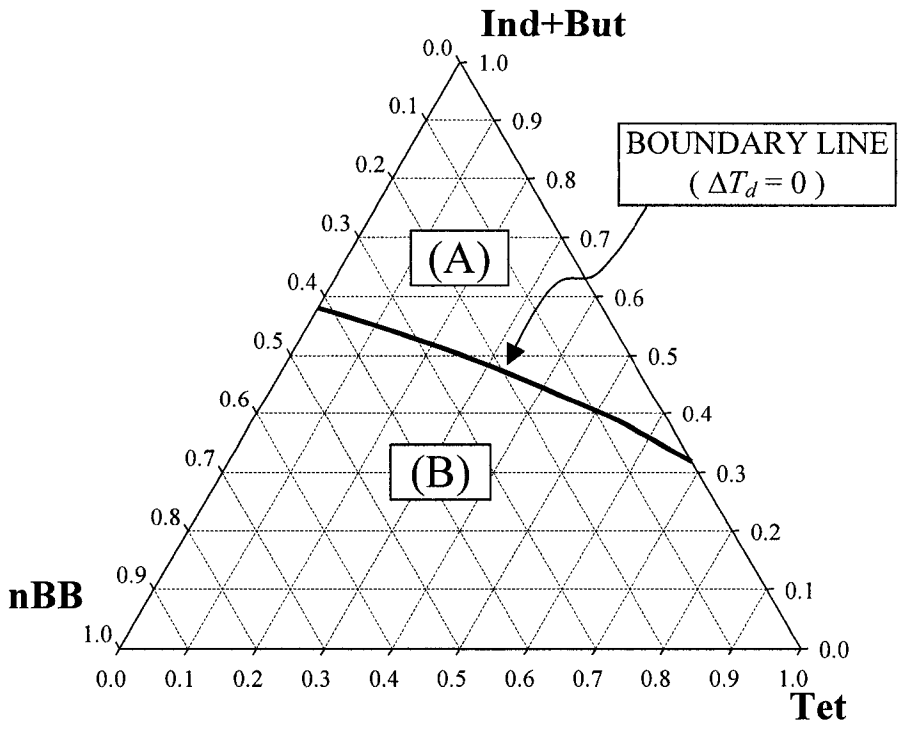

Figure 5.1. Boundary for aerosol formation at typical operation conditions Reaction temperature 530 °C, total pressure 265 kPa, reaction time 11.5 s, steam present, and olefin to diolefin ratio of 9

5.2. TRENDS OBSERVED FROM SIMULATIONS

In this section we evaluate the effect that the process conditions and the olefin to diolefin ratio have on the likehood of forming aerosols due to vapour phase chemical reactions. In order to determine the sensitivity to each process variable, we have selected the extreme conditions for the variable under study and an average or typical process value of the rest of the variables. Appendix F compiles the results for every set of conditions shown in this chapter. In the appendix, the conversion of the reactants and the dew point for several points along the boundary locus are also presented.

5.2.1 EFFECT OF TIME OF REACTION

Figure 5.2 shows the boundary locus for 6 seconds and for 17 seconds.

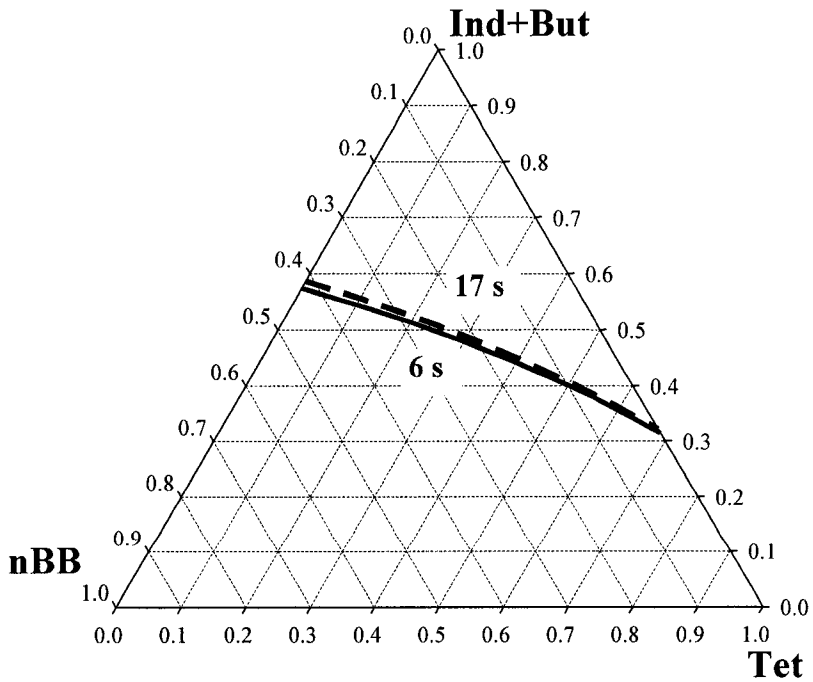

Figure 5.2. Effect of the time of reaction on the locus for aerosol formation
Reaction temperature 530 °C, total pressure 265 kPa, wet, and O/DO ratio of 9

The data of Figure 5.2 clearly show that the boundary for aerosol formation is insensitive to the time of reaction. This is due to the extent of conversion, which was below 10 % for all of the components, except butadiene in the longest reaction time. Also, the addition and cracking reactions tend to compensate in the two position of the time. The direct consequence of the insensitivity to reaction time is that the residence time distribution is not a significant factor in the model calculations.

Another important observation that will be appearing also in all of the following ternary diagrams is that the olefin plus diolefin content requirements for aerosol to form, increase with the n-butylbenzene content, so that the boundary trends lower from left to right in the ternary diagram. Tetralin behaves more like an inert compound in the mixture, with very low levels of conversion in comparison to n-butylbenzene as shown above. However, this simulation is conservative, since it does not allow coupling of the free radical reactions. If coupling reactions were allowed n-butylbenzene would accelerate the cracking of tetralin (Rebick, 1983). In this case, the two ends of the boundary would be the same, but the curve would show an increase in the olefin requirements at low concentration of n-butylbenzene, i.e. circa the binary mixture of tetralin and Ind+But. This shift would increase the curvature of the boundary in the concave-down direction, relative to the results of Figure 5.2.

5.2.2 EFFECT OF STEAM

Figure 5.3 shows the boundary locus with steam present and absent from the reaction mixture. The presence of steam dilutes the reaction mixture. At all hydrocarbon compositions, more Ind+But is needed in order to form aerosol in the presence of steam, in comparison with the dry case. The addition reactions are second order reactions, so that in the presence of steam the partial pressure of the olefin and diolefin are reduced and hence a feed with higher content of Ind+But is required to increase the dew point. The amount of steam used for this calculation corresponds to the actual process, i.e. the curve with steam present in Fig. 5.3 would represent the boundary for the typical working conditions of the fluid coker.

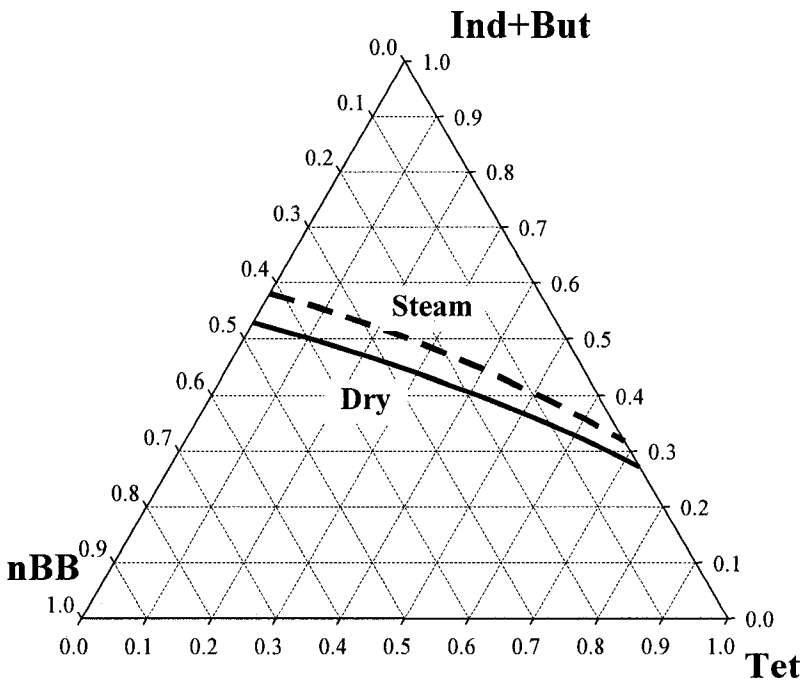

Figure 5.3. Effect of steam on the boundary for aerosol formation
Reaction temperature 530 °C, total pressure 265 kPa, reaction time 11.5 s, and olefin to diolefin ratio of 9

5.2.3 Effect of Pressure

The boundary was more sensitive to an increase in reactor pressure, as illustrated in Fig. 5.4. The same concept explained for the effect of steam applies for pressure. The addition reactions are favoured by the increase in the partial pressure of the hydrocarbon mixture. Hence, the concentration of olefins to obtain an increase in the dew point temperature at 350 kPa, for any combination of n-butylbenzene and tetralin is much lower than that at 100 kPa.

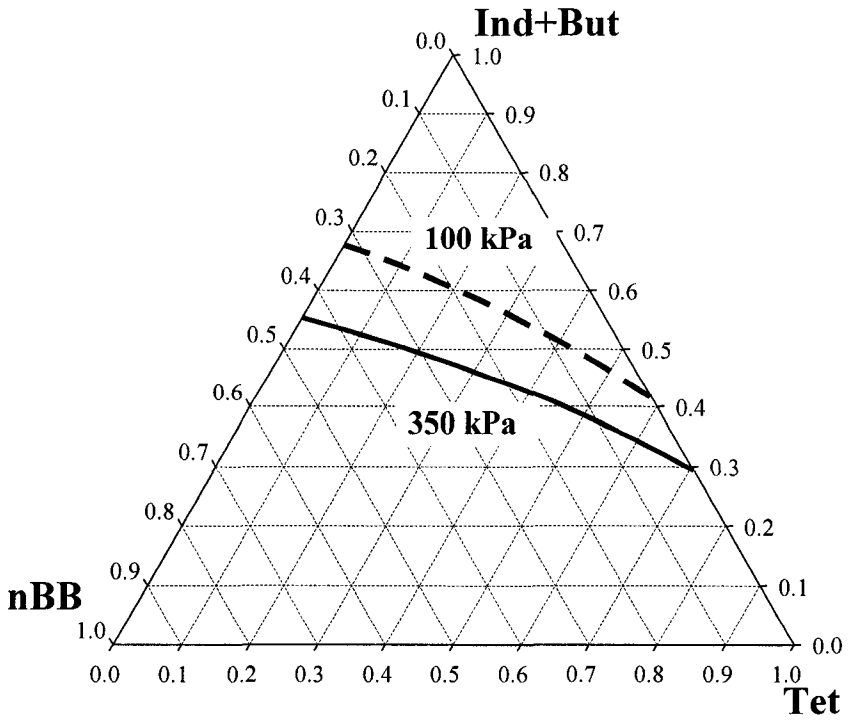

Figure 5.4. Effect of pressure on the boundary for aerosol formation
Reaction temperature 530 °C, reaction time 11.5 s, wet, and olefin to diolefin ratio of 9

5.2.4 Effect of Temperature

The effect of reactor temperature is illustrated in Figure 5.5. The increase of the temperature favours the cracking reactions, relative to the addition. The extent of conversion increased 3.4 and 2.9 times for tetralin and n-butylbenzene, and 1.8 times for 1,3-butadiene and indene, as the temperature increased from 510 to 540 °C. Hence, the olefin and diolefin content required is higher for an increase in the dew point at 540 °C. The fact that aerosol is expected more likely to be formed at lower temperatures agrees with Watkinson et al. (2002), however they attributed the fouling deposits in their reactor apparatus to purely physical condensation. Their argument is valid because they carried out the coking reactions in a dense bed at 540 °C, and then varied the temperature of the cyclone and cyclone outlet. Since their vapour mixture was close to the dew point, as soon as it cooled down in presence of enough nuclei condensation is expected. In the actual process the temperature of the cyclone is higher than the temperature of the dense bed, thanks to the scouring coke that is fed at the inlet of the cyclones.

On the other hand, the formation of diolefins corresponds to secondary products of cracking reactions; hence at higher temperatures in the actual mixture more formation of diolefins is expected. The simple model used in this study did not include the formation of olefins and diolefins; therefore, this trend was not included in the results. With the increase of diolefin content, the boundary in the ternary diagram at the higher temperature is expected to move down, i.e. requiring less olefin and diolefin at the beginning of the reaction. The formation of diolefins

would tend to reduce the sensitivity of the boundary to the effect of reaction temperature.

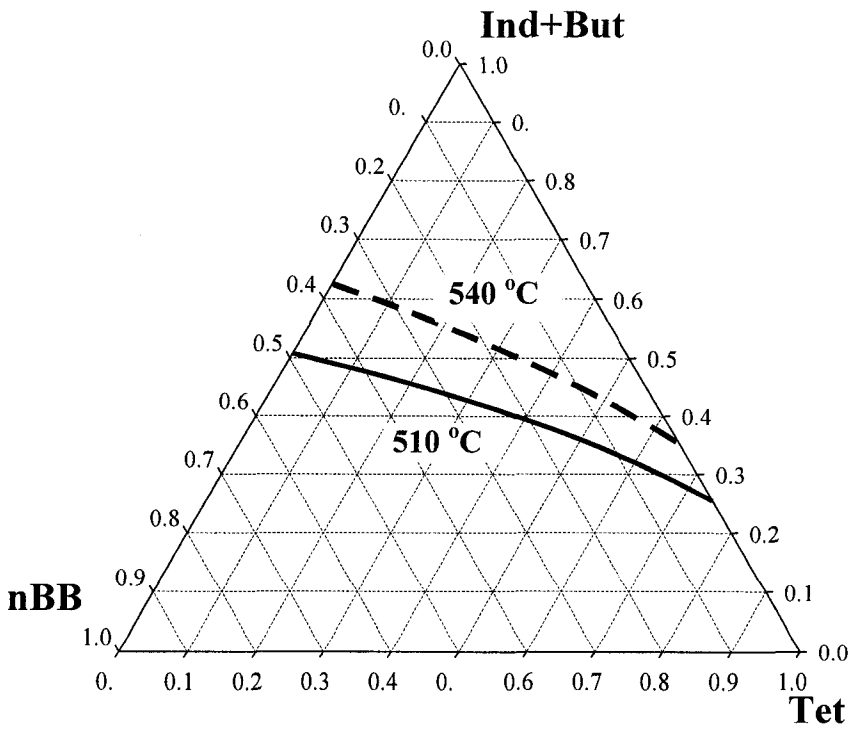

Figure 5.5. Effect of temperature on the boundary for aerosol formation
Total pressure 265 kPa, reaction time 11.5 s, wet, and olefin to diolefin ratio of 9

5.2.5 Olefin to Diolefin Ratio

The olefin to diolefin ratio is an important variable for the formation of aerosol in the coking process, but the formation of these species was not included it the simplified reaction model. The characteristics of the fluid coker feed and the severity of the reactions can change the olefin and diolefin content. For example, diolefin compounds are secondary products of cracking reactions, which can be increased if the content of paraffins in the feed of the fluid coker is high. If the feed

is highly aromatic, then the diolefin content will be lower. The influence in temperature was discussed above; the higher the temperature the more severe the reactions conditions will be, giving more potential to form diolefin compounds.

Figure 5.6 shows the boundaries corresponding to O/DO equal to 9 and 14. The olefin to diolefin ratio of 14 was taken from the olefin and diolefin content of the actual mixture when neglecting the contribution of the coker gas oil. Figure 5.6 shows that less Ind+But is needed when the O/DO ratio is lower, due to the higher concentration of diolefins that accelerates the addition reactions. Given that the olefin and diolefin concentrations were estimated from the actual reactor, the data of Figure 5.6 suggest that the model gives a worst-case prediction for the aerosol at a ratio of 9. Given that the actual ratio in the outlet would be closer to 14, based on the bases of the analytical techniques, the use of a ratio of 9 compensates to some extent for the consumption of diolefin in the reactor by addition reactions. The diolefins are reaction intermediates, generated by cracking of olefins and consumed by addition reactions, and they could only be modeled with certainty by developing a much more complex kinetic model for both the liquid and vapour phase reactions.

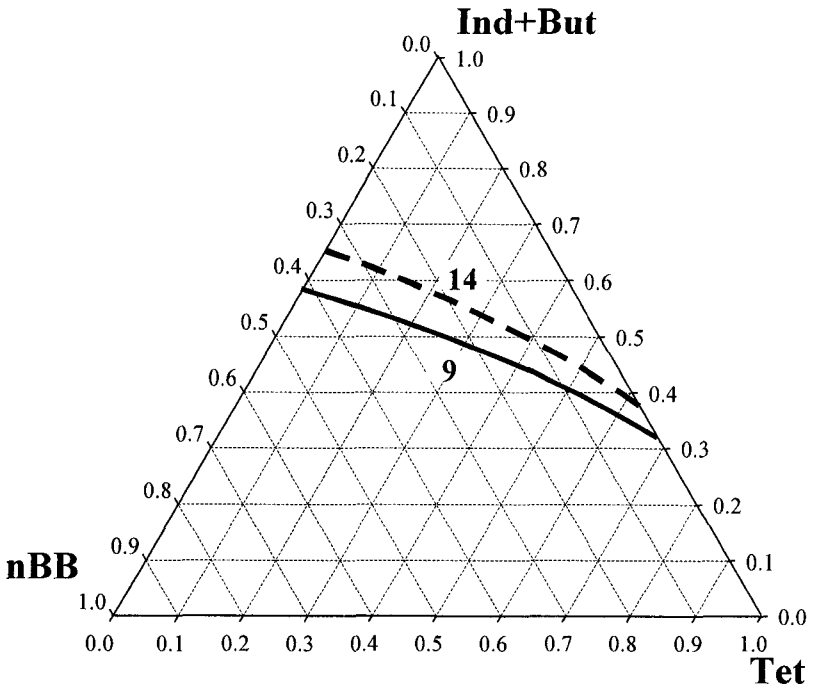

Figure 5.6. Effect of olefin to diolefin ratio on the boundary for aerosol formation

Reaction temperature 530 °C, total pressure 265 kPa, reaction time 11.5 s, and wet

5.3. MODEL REACTOR MIXTURE AS A REPRESENTATION OF COKER OPERATION

The bitumen that feeds the fluid coker is a complex mixture of hydrocarbons that is hard to analyze comprehensively. In addition, the vapour mixture generated in the coking reaction is very different from that of the feed. Furthermore, the levels of conversion of most of the components in the model mixture are low at the vapour phase reactor conditions. Consequently the final products from the fluid coker are the best approximation to the initial vapour phase mixture.

The approach taken in the simulations is to consider the most conservative case, i.e. the simulations are designed maximize the possibilities of forming aerosol. The estimated boundaries for aerosol formation are based on the most extreme conditions for comparison to the actual process.

Having chosen n-butylbenzene as the main cracking material, in the model we do not consider dealkylation reactions, which would increase the formation of methane. Methane represents ca. 15 mol% of the product mixture of the actual process. For the most severe conditions in our simulations, the methane content did not exceed 1 mol%. The more methane content in the product vapour, the less the possibility of forming aerosol. Also, the alkyl chain of the nBB only possesses 4 carbons, but in the actual feed mixture the average chain length is 8 carbon atoms according to estimation of Gray et al. (1992). Longer alkyl chains will reduce the chances of forming aerosols, since they are more reactive for cracking as shown by

Smith and Savage (1991). The number of aromatic rings also influences the reactivity of the alkyl aromatic. Behar et al. (2002) compared their data of cracking of dodecylbenzene with the data of Smith and Savage (1991) of cracking of dodecylpyrene, and found that more aromatic rings favour cracking reactions. Gray et al. (1992) reported an average number of rings of 2 while nBB only has one aromatic ring. In conclusion, n-butylbenzene is a conservative model for cracking reactions.

Coupling of free radical reactions was not allowed in this study. For this reason, tetralin conversion is lower than similar compounds would give in the actual reaction mixture, as discussed previously. Also, hydrogenation of olefins by hydrogen transfer from tetralin, that would diminish the addition reactions, was not allowed either.

The addition reactions taken into consideration were only the reaction of 1,3-butadiene with indene and the inevitable dimerization of 1,3-butadiene. 1,3-Butadiene will readily react with any olefin present in the mixture. Reactions with small olefins, like ethylene and/or propylene, will cause a decrease in the concentration of butadiene available for reaction with indene. The latter reaction will contribute much more significantly to aerosol formation than the addition to the smaller olefins. On the other hand, the steric effect of olefins much larger than indene in the actual mixture would hinder the addition reaction. Consequently, our simulations consider the worst case for addition reactions of diolefins by maximizing the reaction rate, relative to the more complex reactants in the actual

vapour mixture, and by excluding reactions with the light olefins that are abundant in the vapour phase to maximize the increase in the dew point due to addition of butadiene.

The presence of hydrogen sulphide in the vapour phase has also a significant effect on cracking reactions. H_2S acts as a catalyst for the hydrogen-transfer reaction step, hence accelerating the rate of cracking (Rebick, 1980). By ignoring this catalytic effect, we give a more conservative sense to the results.

The fact that the temperature of the coker in the diluted phase is higher (since the hot coke is fed in this section) will accelerate the cracking reactions but also generate more diolefins. Diolefins are secondary reaction products; hence to be formed they need two breakings, which will generate not two components from a single alkyl chain but at least three. This makes the mixture even more diluted and less prone to form aerosols. In conclusion, even at higher temperatures cracking reactions are predominant.

All of the above arguments in summary support the conclusions that the simulations carried in this work will give a worst-case or conservative estimate of the boundary for aerosol formation. The above arguments all suggest that the actual boundaries would occur at a higher concentration of olefin plus diolefin. Margins of error for the simulations are not presented here, but the results shown in the ternary diagrams represent the maximum tendency for aerosol formation, i.e. they show the minimum amount of olefin plus diolefins that shall be present in the vapour phase mixture of the fluid coker to give formation of aerosol under the

given conditions. When comparing the most conservative case with the actual operations we can draw a reliable conclusion regarding the likehood of forming aerosol. This concept can be expanded and adapted to other thermal cracking processes.

5.4. COMPARISON OF BOUNDARIES FOR AEROSOL FORMATION TO ACTUAL COMPOSITION

In order to determine the actual operating point of the commercial reactor in the ternary diagram, we need to estimate the concentrations of the three main reaction lumps; alkyl aromatics, hydroaromatics and olefins plus diolefins. The concentration of alkyl side chains on aromatics can be estimated from nuclear magnetic resonance (NMR) spectroscopy. Gray et al. (1992) reported gamma methyl carbons for the product fractions from a laboratory batch coking reactor using Athabasca vacuum residue as feed. The gamma methyl carbons are terminal carbons in aliphatic chains of at least 5 carbons. These values were used to estimate the alkyl aromatic content in the vapour phase of the fluid coker, in a ratio 1:1. The values reported in moles/100 g. were 0.786, 0.546, 0.272, and 0.364 for naphtha, LGO, HGO, and residue, respectively. These values combined with the information on the fluid coker composition (Table 2.2), the assay data (Table 2.5), and in section 2.4 regarding the residue fraction, we estimated that the alkyl aromatic content in the dry mixture is equal to 53 mol%.

In figure 5.7 the composition in the actual mixture (olefin plus diolefin, see 5.1.1 and alkyl aromatic), represented by a dot, is shown against the boundary locus for the most favourable conditions for aerosol formation in the simulations. The composition of olefins plus diolefins estimated from the commercial operation data corresponds to a maximum, being the actual value lower than 31 mol%. The olefin

to diolefin ratio used for this calculation corresponds also to the most favourable value for aerosol formation.

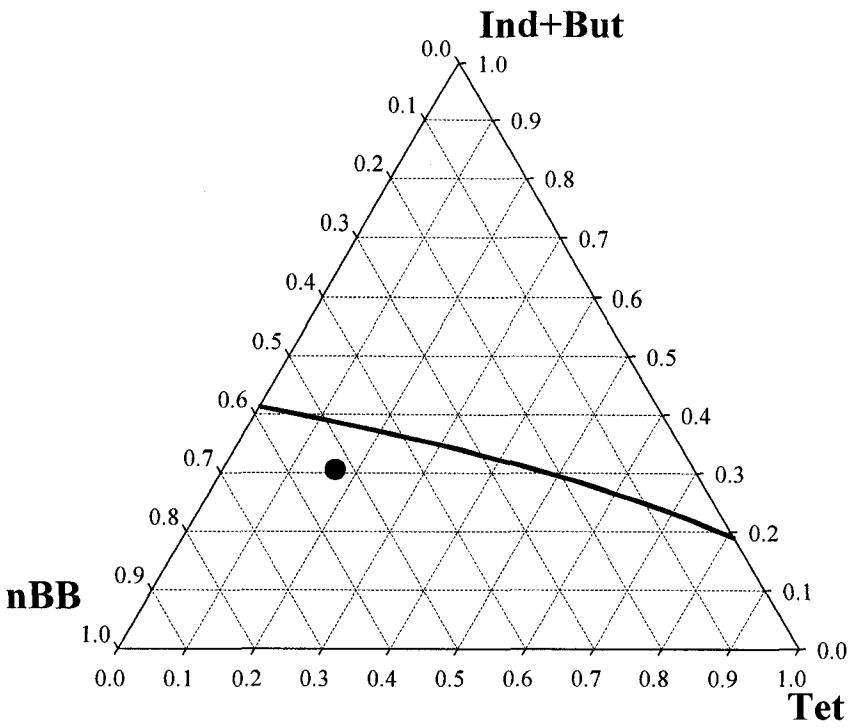

Figure 5.7. Comparison of actual composition to worst-case boundary for aerosol formation

Reaction temperature 510 °C, total pressure 350 kPa, reaction time 6 s, dry, and olefin to diolefin ratio of 9. The dot symbolizes the commercial operations.

On the other hand, the gamma methyl carbons represent aliphatic chains prone to undergo cracking reactions that will give a more diluted mixture and with smaller species; hence, given a significant reduction of the likehood of forming aerosol. With this in mind the alkyl aromatic content or the content of the material prone to crack would be higher than the estimate of 53 mol % given in the figure. In addition, if coupling of the free radicals were allowed the cracking of tetralin would have been accelerated giving a more pronounce change in the boundary

curve, i.e. the actual minimum alkyl aromatic requirement for 31 mol% of olefins plus diolefins to avoid the formation of aerosols is even less than 25 mol% that can be observed in Figure 5.7. Furthermore, alkyl aromatics are dominant in the product mixture and the actual composition will be well above the worst-case threshold of 25 mol%. Hence, we can conclude that heterogeneous condensation due to vapour phase chemical reaction is unlikely according to the approach taken in this work.

5.5. IMPLICATIONS FOR REACTOR OPERATIONS

The sensitivity analysis of the reactor operating conditions indicates that higher reactor temperatures will reduce the chance of forming of aerosols due to vapour phase chemical reactions. The lower the hydrocarbon partial pressure, the more inhibited the second order addition reaction will be. Also, the feed to the fluid coker will play an important role in the vapour-phase composition. A high content of paraffinic materials will tend to produce more diolefins that will undergo addition reactions and increase the possibilities for aerosols to form.

Last section concluded that aerosol formation by vapour phase chemical reaction is unlikely. However, aerosol can be formed in the dense bed due to other mechanisms, such as local cooling, then the resulting liquid droplets would have a much higher concentration of reactive components than the vapour phase. This abrupt increase in the concentration in the liquid phase would rise the free radical addition reactions (Wu et al., 1996), Diels-Alder reactions and polymerization reactions, producing more rapid addition and cross-linking of the liquid material. The resulting polymerized material would then be difficult to re-evapourate even in the free board. These particles might end up fouling the reactor walls and the cyclone outlet producing fouling that will ultimately produce shut down of the equipment due to the increase in back pressure, or end up in the hydrotreater were plugging and deactivation of the catalyst will occur.

The fouling problem in the fluid coker can be reduced if the condensable species or precursors are eliminated from the vapour phase. One alternative would

be Kelvin condensation, which implies that the vapour pressure of a liquid contained in a small diameter capillary is lower than the vapour pressure in the bulk. Hence, recalling Eq. 2.1, the saturation ratio is equal to the ratio between the actual pressure of the vapours and the vapour pressure at the dew point. Consequently, by using highly porous material, we can induce condensation inside the pores, avoiding condensation to form aerosol in the bulk vapour stream, where the sizes of the particles formed will be more difficult to scrub out.

6. CONCLUSIONS AND RECOMMENDATIONS

6.1. CONCLUSIONS

The literature survey in aerosol formation, trapping, and its implications in bitumen upgrading in Chapter 2 suggested that the formation of aerosol liquids could be an important process in fluid cokers. The liquid material formed can undergo much faster addition and polymerization reactions due to the increase in the density. These reactions would make aerosol difficult to re-evaporate, and due to the small size of these particles, they would pass from the reactor into the coker cyclones, the coker stripper, and downstream units.

A simulation approach using model compounds to represent the complex vapour phase mixture in the fluid coker has been developed to evaluate the likehood of forming aerosol by heterogeneous condensation due to vapour phase chemical reaction.

The requirement of olefins plus diolefins for the reacting mixture with n-butylbenzene (no tetralin present) increased in 11 mol%, when increasing the temperature from 510 to 540 ^{o}C. Meanwhile, a 12 mol% increase in the olefins requirement was obtained when reducing the total pressure from 350 to 100 kPa. Hence we conclude that in order to reduce the chance of forming aerosol due to vapour phase chemical reaction: temperature of the fluid coker should be high and the pressure of the mixture low. The likehood of forming aerosol is insensitive to the reaction time.

Aerosol formation by heterogeneous condensation due to vapour phase chemical reactions is not favourable at the composition of the vapour phase in fluid cokers operating with Athabasca bitumen as feed. This conclusion was based on the most conservative estimates that maximize the probability of forming aerosols, and to identify the minimal content of olefins plus diolefins required based on the results from the sensitivity analysis.

6.2. RECOMMENDATIONS

Aerosol formation by heterogeneous condensation needs further study to consider the other possible mechanisms. We suggest the examination of non-isothermal conditions due to the presence of cold spots in the fluid coker. The spraying nozzles and the steam injection areas should be studied using an adaptation of the methodology provided in this thesis.

Kelvin condensation phenomenon might be beneficial to avoid formation of aerosols in the bulk of the fluid coker, producing the condensation inside a porous material. These porous materials or particles could be of a certain size that can be easily removed from the vapour stream before they go into down stream equipments or units. This approach would be able to suppress the dew point of the vapour mixture.

LIST OF REFERENCES

American Society for Testing and Materials (ASTM), "Manual of Hydrocarbon Analysis", 3rd ed. (1977)

Behar, F., F. Lorant, H. Budzinski, and E. Desavis, "Thermal Stability of Alkylaromatics in Natural Systems: Kinetics of Thermal Decomposition of Dodecylbenzene", Energy & Fuels, 16 (4) 831 – 841 (2002)

Base, T.E., E.W. Chan, R.D. Kennett, and D.A. Emberley, "Nozzle for atomizing liquid in two phase flow", U.S. Patent # 6,003,789. December 21, 1999

Bredael, P. and D. Rietvelde, "Identification of Pyrolysis Products of Cis-Decalin", *J. Chromatography*, 192 (1), 216 – 221 (1980)

Burkholz, A., "Droplet Separation", VCH Publishers, Germany (1989)

Calvert, S., S. Yung, and J. Leung, "Entrainment Separators for Scrubbers – Final Report", U.S. Environmental Protection Agency, Washington D.C. (August 1975). EPA-650/2-74-119-b.

Cents, A.H.G., S.R.A. Kersten, and D.W.F. Brilman, "Gas Phase RTD Measurement in Gas and Gas-Solids Reactors Using Ultrasound", *Ind. Eng. Chem. Res.*, **42** (22) 5506 – 5515 (2003)

Christensen, K.A. and H. Livbjerg, "A Plug Flow Model for Chemical Reactions and Aerosol Nucleation and Growth in an Alkali-Containing Flue Gas", *Aerosol Sci. & Tech.*, **33**, 470–489 (2000)

Coker, K., "Understand cyclone design", *Chem. Eng. Prog.* **89** (12), 51 – 55 (1993)

CRC Handbook of Chemistry and Physics, Edited by D.R. Lide, 84th ed., CRC Press Inc, Boca Raton (2003 – 2004)

Davis, H.G. and K.D. Williamson, "Product Inhibition in the Pyrolysis of Paraffinic Hydrocarbons" in "Thermal Hydrocarbon Chemistry", Edited by A.G. Oblad, H.G. Davis, and R.T. Eddinger, *Advances in Chemistry Series 183*, American Chemical Society Publications, Washington, D.C. (1979). 41 – 66

Doue, F. and G. Guiochon, "Formation of Alkanes in Pyrolysis of n-Hexadecane - Effect of an Inert Gas on Decomposition of Alkyl Radicals", Canadian Journal of Chemistry, **47** (18) 3477 (1969)

Freund H. and W.N. Olmstead, "Detailed Chemical Kinetic Modeling of Butylbenzene Pyrolysis", *Int. J. Chem. Kin.*, **21**, 561 – 574 (1989)

Friedlander, S.K., "Smoke, Dust and Haze, Fundamentals of Aerosol Behavior", Jonh Wiley & Sons, Inc. (1977)

Friedlander, S.K., "Smoke, Dust and Haze, Fundamentals of Aerosol Behavior", Jonh Wiley & Sons, Inc. (2000)

Froment, G.F., "Coke Formation in the Thermal Cracking of Hydrocarbons", *Rev. Chem. Eng.*, 6 (4), 293 – 328 (1990)

Froment, G.F., B.O. Van de Steene, and O.Sumedha, "Selectivities and Yields in Cocracking Ethane and Propane", *Oil & Gas J.*, **77** (16), 87 – 90 (1979)

Froment, G.F., B.O. Van de Steene, P.J. Vander Berghe, and A.G. Goossens, "Thermal-Cracking of Light-Hydrocarbons and Their Mixtures", *AIChEJ*, **23** (1), 93 – 106 (1977)

Ghadiri, M., J.P.K. Seville, and R. Clift, "Fluidize Bed Filtration of Gases at high Temperatures", *Trans IchemE*, **71**, 371-381 (July 1993)

Gray, M, "ChE 522: Hydrocarbon Fluid Properties and Processing", Department of Chemical Engineering, University of Alberta, (2003)

Gray, M., A.Z. Krzywicki, and S.E. Wanke, "Chemical Transformation during rasid Upgrading: Catalytic and Thermal", Report to CANMET, SSC # 06SQ.23440-7-9011 (1992)

Gray, M., W. McCaffrey, I. Huq, and T. Le, "Kinetics of Cracking and Devolatilization during Coking of Athabasca Residues", (2003), In press.

Hidy, G. M., "AEROSOLS, An Industrial and Environmental Science", Academic Press, Inc. Orlando (1984)

Hillebrand W., W. Hodek, and G. Kolling, "Steam Cracking of Coal-Derived Oils and Model Compounds.1. Cracking of Tetralin and T-Decalin", *Fuel*, **63** (6), 756 – 761 (1984)

Joback, K.G., M.S. thesis in Chemical Engineering, Massachuserrs Institute of Technology, Cambridge, Mass., June (1984)

Khorasheh F., M. Sc. Thesis: "Structural Characterization of Alberta Gas Oils", Department of Chemical Engineering, University of Alberta, Spring 1986.

Khorasheh, F. and M.R. Gray, "High-Pressure Thermal-Cracking of n-Hexadecane in Tetralin", *Energy & Fuels*, **7** (6), 960-967 (1993a)

Khorasheh, F. and M.R. Gray, "High-Pressure Thermal-Cracking of n-Hexadecane", *Ind. Eng. Chem. Res.*, **32** (9), 1853 – 1863 (1993b)

Khorasheh, F. and M.R. Gray, "High-Pressure Thermal-Cracking of n-Hexadecane in Aromatic Solvents", *Ind. Eng. Chem. Res.*, **32** (9), 1864 – 1876 (1993c)

Kistiakowsky, G.B. and W.W. Ransom, *J.Chem. Phys.*, **7**, 725 (1939)

Koch-Otto York® Separation Technology, Otto York™. "Mist Elimination", Bulleting ME5601-4, USA (2002), from www.koch-ottoyork.com.

Mallory, D.G., D.A. Mehta, R.G. Moore, and S. Richardson, "The Role of the Vapour Phase in Fluid Coker Cyclone Fouling: Part 1. Coke Yields", *Can. J. Chem. Eng.*, **78**, 330 – 336 (April, 2000)

Mushrush, G.W., W.M. Stalick, G.D. Lacy, and R. Yaghoubi, "Pyrolysis of Tetralin at 450°C", *J. Analitical and Applied Pyrolysis*, **14**, 17 – 23 (1988)

Nohara, D. and T. Sakai, "Addition-Reaction of Allyl Radical and Butadiene", *Ind. Eng. Chem. Res.*, **27** (10) 1925 – 1929 (1988)

Nohara, D. and T. Sakai, "Kinetic Study of Cycloaddition of Allyl Radical to Acetylene", *Ind. Eng. Chem. Fundam.*, **19**, 340 (1980)

Nohara, D. and T. Sakai, "Kinetic Study of Model Reactions in the Gas Phase at the Early Stage of Coke Formation", *Ind. Eng. Chem. Res.*, **31** (1) 14 – 19 (1992)

Peddy, R.V.C., V.J. Prasad, and B.D. Bhatt, "Structural Studies of Feedstocks of Petrochemcal Industry using NMR Spectroscopy", *Indian J. Technology*, **30**, 458–462 (Sep. 1992)

Peng, D.Y. and D.B. Robinson, "A New Two-Constant Equation of State", *Ind. Eng. Chem. Fundam.*, **15** (1), 59 - 64 (1976)

Perry, R. and C.H. Chilton, "Perry's Chemical Engineer's Handbook", 5th ed., McGraw-Hill, Inc. (1973). Section 18 and 20.

Perry, R. and D.W. Green, "Perry's Chemical Engineer's Handbook", 7th ed., McGraw-Hill, Inc. (1999). Section 14 and 17.

Pilinis, C. and J.H.Seinfeld, "Continued development of a general equilibrium model for inorganic multicomponent atmospheric aerosols", 11), 2453–2466 (1987).

Pilinis, C., J.H. Seinfeld, and C. Seigneur, "Mathematical modeling of the dynamics of multicomponent atmospheric aerosols", *Atmospheric Environment*, **21** (4), 943–955 (1987)

Pitzer, K.S., "The Volumetric and Thermodynamic Properties of Fluids .1. Theoretical Basis and Virial Coefficients", *J. Am. Chem. Soc.*, **77**(13), 3427 – 3433 (1955)

Poutsma, M.L., "Free Radical Thermolysis and Hydrogenolysis of Model Hydrocarbons Relevant to Processing of Coal", *Energy & Fuels*, **4** (2) 113 – 131 (1990)

Rebick, C., "Hydrogen Transfer Catalysis in Hydrocarbon Pyrolysis" in "Frontiers of Free Radical Chemistry", Edited by W.A. Pryor, Academic Press Inc., New York (1980), 117 – 137

Rebick, C., "Pyrolysis of Heavy Hydrocarbons" in "Pyrolysis: Theory and Industrial Practice", Edited by L.F. Albright, B.L. Crynes, and W.H. Corcoran. Academic Press, Inc. New York (1983), 69 – 87

Riedel, L., *Chem. Eng. Tech.*, **26**, 83 (1954)

Rowley D. and H. Steiner, *Discussions of the Faraday Society*, **10,** 198 (1951)

Sakai, T., "Thermal Reaction of Olefins and Diolefins, and Formation of Aromatics" in "Pyrolysis: Theory and Industrial Practice", Edited by L.F. Albright, B.L. Crynes, and W.H. Corcoran. Academic Press, Inc. New York (1983), 89 – 116

Sakai, T., K. Soma, Y. Sasaki, H. Tominaga, and T. Kunugi, "Secondary Reactions of Olefins in Pyrolysis of Petroleum Hydrocarbons" in "Refining Petroleum for Chemicals", *Advances in Chemistry Series 97*, American Chemical Society Publications, Washington, D.C. (1970), 68 – 91

Schaber, K. "Aerosol Formation in Absorption Processes", *Chem. Eng. Sci.* **50** (7), 1347-1360 (1995)

Schaber, K., J. Korber, O. Ofenloch, R. Ehrig, and P. Deuflhard, "Aerosol Formation in Gas-Liquid Contact Devices-Nucleation, Growth and Particle Dynamics", *Chem. Eng. Sci.* **57**, 4345-4356 (2002)

Schifftner, K.C., and H.E. Hesketh, "Wet Scrubbers, The Environmental and Energy Handbook Series", Ann Arbor Science Publishers Inc., Ann Arbor(1983)

Smith C.M. and P.E. Savage, "Reactions of Polycyclic Alkylaromatics. 1. Pathways, Kinetics, and Mechanisms for 1 -Dodecylpyrene Pyrolysis", *Ind. Eng. Chem. Res.*, **30** (2) 331 – 339 (1991)

Soave, G., "Equilibrium Constants from a Modified Redlich-Kwong Equation of State", *Chem. Eng. Sci.*, **27** (6), 1197 (1972)

Tomaides, M. and K.T. Whitby, "Generation of Aerosols by Bursting of Single Bubbles" in "FINE PARTICLES, Aerosol Generation, Measurement, Sampling, and Analysis", Edited by LIU, B.Y.H., Academic Press, Inc. New York (1976), 235-252

Universal Oil Products (UOP), Laboratory Test Methods for Petroleum and its Products, UOP Process Division, Des Plaines, IL (1965)

Wankat, P.C., "Equilibrium Staged Separations: Separations in Chemical Engineering", Prentice Hall, New York (1988).

Watkinson A.P., J. Xu, and I.C. Rose, "Vapour Phase Fouling in Bitumen Cracking Applications" in "Heat Exchanger Fouling-Fundamental Approaches and Technical Solutions", H. Muller-Steinhagen (Ed.), PUBLICO Publications, Essen, Germany, pp 269 - 274 (2002)

Wexler, A. and J.H. Seinfeld, "Modeling Urban And Regional Aerosols. 1. Model Development", *Atmospheric Environment*, **28** (3), 531-546 (1994)

Yui, S., "Removing Diolefins from Coker Naphtha Necessary before Hydrotreating", *Oil & Gas Journal*, **97** (36), 64 – 68 (1999)

Yui, S.M. and S.H. Ng, "Hydrotreating of Bitumen-Derived Coker HGO and Evaluation of Hydrotreated HGOs as Potential FCC Feeds Using Microactivity Test Unit", *Energy & Fuels*, **9**, 665 – 672 (1995)

Yui, S.M., "Hydrotreating of Bitumen-Derived Coker Gas Oil: Kinetics of Hydrodesulfurization, Hydrodenitrogenation, and Mild Hydrocracking, and Correlations to Predict Product Yield and Properties", *AOSTRA Journal of Research*, **5** (3), 211 – 224 (1989)

Zhang, K.M. and A.S. Wexler, "Modeling the number distributions of urban and regional aerosols: theoretical foundations", *Atmospheric Environment*, **36**, 1863–1874 (2002)

APPENDIX A
ALGORITHMS

This appendix shows in Fig. A.1 the main algorithm developed to construct the boundary locus for aerosol formation. The algorithm basically starts with the reading of the operating conditions and the initial composition of one of the reactants (tetralin), the composition of n-butybenzene is assumed and the composition of 1,3-butadiene plus indene is calculated. Once a value of n-butylbenzene comply the condition of $\Delta T_d = 0$, the initial compositions are saved and an increment in the tetralin composition takes place to repeat the routine until the locus is completed.

Three subroutines are present in up case and italics font in Fig. A.1 the first is *KINETICS* that refers to the MATLAB listings A.1 or A.2 (PYROCOND_PFR or PYROCOND_CSTR). The second is *VLE* this refers to the dew point calculation executed by HYSYS. The third is *LAGRANGE_INTERP*, which interpolates the three values of n-butylbenzene molar fraction and their corresponding ΔT_d, for a ΔT_d value of zero; hence getting a better estimation of the initial composition at the boundary for the next iteration.

Followed you can find the listing for the MATLAB code used for the executing the "KINETICS" routine. Listing A.1 shows the function PYROCOND_PFR that was the code used for solving the set of ordinary differential equations for the plug flow reactor model. Listing A.2 shows the code for the solution of the system of non-linear equations of the continuous stirred tank

reactor model evaluated in Appendix B, this listing also include the MATLAB function with the system of equations and the Jacobian of the system for solving it using the Newton's method.

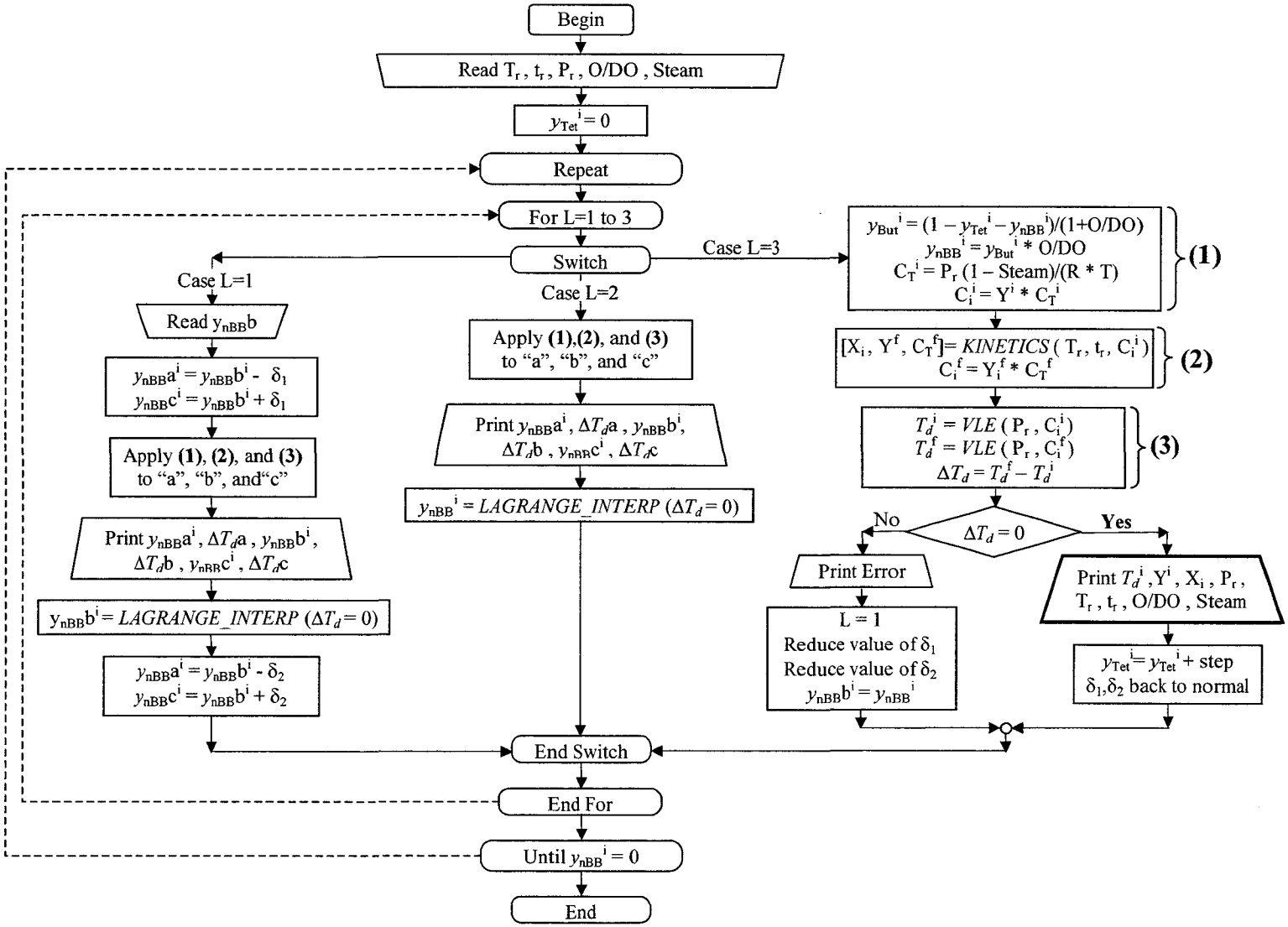

Figure A.1. General algorithm for constructing the boundary locus for a given set of conditions

Listing A.1. MATLAB code for evaluating the kinetics of the PFR model

```
%X   Vector of conversion through out the reactor
%v   Vector of the length of the reactor
%Y   Matrix of the molar fraction of the species at any given position in
%the reactor
%Moles  Vector of total moles during the reaction
%K   Vector with the rate constants
%Co  Vector of initial concentration of the species
%F   Matrix of molar flow with position of the reactor

function [X,v,Y,Moles]= PyroCond_PFR(Condition, ICond,K);
close all;
T = Condition (1)+273.15;
TiempoX = Condition (3); Flag2 = Condition (2);
if Flag2 == 0
    Co = [ICond(1) ICond(2) ICond(4) ICond(3)  0   0    0]; %NORMAL
        %[Tetralin nBBenzen Butadien Indene  VCH 4HF XnBB]XnBB=nBB reacted
else
    Co = [ICond(2)     0    ICond(4) ICond(3)  0   0    0]; %nBB = 0
        %[Tetralin nBBenzen Butadien Indene  VCH 4HF XnBB]XnBB=nBB reacted
end
Vol = 1e6;                          % Volume of the Reactor Assume, cm^3
Qo = Vol/TiempoX;  % Calc. the initial Vol. Flow for the space time,
cm^3/s
Fo = Co*Qo;                         % Initial Mole Rate
Rg= 8.3145;
P_RT = sum(Co);                     % [mol/cm^3]
Knew (1:2) = K(1:2)*P_RT;           % K Values in mol/(cm^3.s)
Knew (3:4) = K(3:4)*P_RT^2;         % K Values in mol^2/(cm^3^2.s)
int = Vol/1000;                     % Interval
Vspan = 0:int:Vol;
[v,F] = ode45(@dFdV,[Vspan],Fo,[],Knew,Fo(1)); %ODE solver
n = length(v);
XTet = Fo(1)-F(:,1);
XnBB = F(:,7)/0.206;                %Amount of nBB reacted
F(:,7:9) = XTet*[.106      .731      .854 ];
                %7)Naph 8)1,2DHNaph   9)H2
F(:,10:14)= [0.206*XnBB, ...                %10)Propylene
             0.1807*XnBB, ...               %11)Toluene
             0.057*XnBB, ...                %12)Allylbenzene
             0.010*XnBB, ...                %13)Benzene
             0.012*XnBB];                   %14)12DBE
F(:,15:19)= [0.021*XTet + 0.693*XnBB, ...   %15)Styrene
             0.021*XTet + 0.617*XnBB, ...   %16)Ethane
             0.021*XTet + 0.136*XnBB, ...   %17)Ethylene
             0.021*XTet + 0.033*XnBB, ...   %18)Ethylbenzene
             0.073*XTet + 0.094*XnBB];      %19)Methane
for i = 1:4
    if Fo(1,i)==0
        X(1:1001,i) = 0;
    else
        X(1:1001,i) = 1-F(1:1001,i)./Fo(1,i);
    end
end %for
Flag1 = 1;
for i= 1:n
    Moles (i,1)= sum(F(i,:));
    Y (i,1:19)= (F(i,1:19)/Moles (i,1));
end %for
```

```
Xf = X(n,1:4);
Yf = Y(n,1:19)';


% ------------------------------------------------------------------------

% System of ordinary differential equations

function dFdV = dFdV(v,F,K,Fo1)
dFdV = [- K(1)*F(1)/(1.848*Fo1-0.848*F(1)+F(2)+F(3)+F(4)+F(5)+F(6) ...
           +9.898*F(7));                                    %(1)Tetralin
       (- K(2)*F(2) + K(1)*F(1)*0.047)/(1.848*Fo1-0.848*F(1)+F(2)+F(3) ...
           +F(4)+F(5)+F(6)+9.898*F(7));                %(2)Butyl Benzene
       (- 2*K(3)*F(3)^2 - K(4)*F(3)*F(4))/(1.848*Fo1-0.848*F(1)+F(2) ...
           +F(3)+F(4)+F(5)+F(6)+9.898*F(7))^2;             %(3)Butadiene
        0.073*K(1)*F(1)/(1.848*Fo1-0.848*F(1)+F(2)+F(3)+F(4)+F(5)+F(6) ...
           +9.898*F(7))-K(4)*F(3)*F(4)/(1.848*Fo1-0.848*F(1)+F(2)+F(3) ...
           +F(4)+F(5)+F(6)+9.898*F(7))^2;                  %(4)Indene
        K(3)*F(3)^2/(1.848*Fo1-0.848*F(1)+F(2)+F(3)+F(4)+F(5)+F(6) ...
           +9.898*F(7))^2;                                 %(5)VCH
        K(4)*F(4)*F(3)/(1.848*Fo1-0.848*F(1)+F(2)+F(3)+F(4)+F(5)+F(6) ...
           +9.898*F(7))^2;                                 %(6)4HF
        0.206*K(2)*F(2)/(1.848*Fo1-0.848*F(1)+F(2)+F(3)+F(4)+F(5)+F(6) ...
           +9.898*F(7))];                               %(7)nBB reacted
```

Listing A.2. MATLAB code for evaluating the kinetics of the CSTR model

```
function [X,Y,Moles,Yo,Qo,Qe]= PyroCondCSTR(Condition, ICond,K);
close all;
T=Condition(1)+273.15; TiempoX=Condition (3); Flag2=Condition (2);
if Flag2 == 0
    Co = [ICond(1) ICond(2) ICond(4) ICond(3)  0   0    0]; %NORMAL
    %  [Tetralin nBBenzen Butadien Indene   VCH 4HF  XnBB] XnBB=nBB
reacted
else
    Co = [ICond(2)     0    ICond(4) ICond(3)  0   0    0]; %nBB = 0
    %  [Tetralin nBBenzen Butadien Indene   VCH 4HF  XnBB] XnBB=nBB
reacted
end
Vol = 1e6;                              % Volume of the Reactor Assume
cm^3
Qo = Vol/TiempoX;   %Calc. the initial Vol. Flow for the space time cm^3/s
Fo = Co*Qo;                             %Initial Mole Rate
Yo = Fo/sum(Fo);
Rg= 8.3145;
P_RT = sum(Co);                         % [mol/cm^3]
Knew (1:2) = K(1:2)*P_RT;   % K Values in mol/(cm^3.s)
Knew (3:4) = K(3:4)*P_RT^2;

%Following the call for the Newton Method
[F,Conv]=Newton_CSTR('Fun_CSTR','Jac_CSTR',(Fo*0.9999)',Fo',Knew,Vol);
                                          %Initial Guess
XTet = Fo(1)-F(1);
XnBB = F(7)/0.206;                      %Amount of nBB reacted
F(7:9) = XTet*[.106      .731      .854 ]';
               %6)Naph 7)1,2DHNaph  8)H2
F(:,10:14)= [0.206*XnBB, ...                %10)Propylene
             0.1807*XnBB, ...               %11)Toluene
             0.057*XnBB, ...                %12)Allylbenzene
             0.010*XnBB, ...                %13)Benzene
             0.012*XnBB];                   %14)12DBE
F(:,15:19)= [0.021*XTet + 0.693*XnBB, ...   %15)Styrene
             0.021*XTet + 0.617*XnBB, ...   %16)Ethane
             0.021*XTet + 0.136*XnBB, ...   %17)Ethylene
             0.021*XTet + 0.033*XnBB, ...   %18)Ethylbenzene
             0.073*XTet + 0.094*XnBB];      %19)Methane
for i = 1:4
    if Fo(1,i)==0
        X(i) = 0;
    else
        X(i) = 1-F(i)./Fo(1,i);
    end
end %for
Flag1 = 1;
Moles = sum(F(:));
Qe = Moles/sum(Co)
Y (1:19,1)= (F(1:19)/Moles )
```

```
% ------------------------------------------------------------------------

%System of non-linear equations

function g = Fun_CSTR(F,Fo,K,V);

Ft = 1.848*Fo(1)-0.848*F(1)+F(2)+F(3)+F(4)+F(5)+F(6)+9.898*F(7)

g(1,1) = (Fo(1)-F(1))/V - K(1)*F(1)/Ft;
g(2,1) = (Fo(2)-F(2))/V + (-K(2)*F(2) + 0.047*K(1)*F(1))/ Ft;
g(3,1) = (Fo(3)-F(3))/V - (2*K(3)*F(3)^2 + K(4)*F(3)*F(4))/Ft^2;
g(4,1) = (Fo(4)-F(4))/V - K(4)*F(3)*F(4)/Ft^2 + 0.073*K(1)*F(1)/Ft;
g(5,1) = F(5)/V - K(3)*F(3)^2/Ft^2;
g(6,1) = F(6)/V - K(4)*F(3)*F(4)/Ft^2;
g(7,1) = F(7)/V - 0.206*K(2)*F(2)/Ft;


% ------------------------------------------------------------------------

%This function creates the Jacobian for the system of equations of the
%CSTR

function Ja = Jac_CSTR (F,Fo,K,V)
Ft = 1.848*Fo(1)-0.848*F(1)+F(2)+F(3)+F(4)+F(5)+F(6)+9.898*F(7);
F7x = 9.898;

Ja (1,1) = - 1/V - (K(1)*Ft + 0.848*K(1)*F(1))/Ft^2;
Ja (1,2) = K(1)*F(1)/Ft^2;
Ja (1,3) = Ja (1,2);
Ja (1,4) = Ja (1,2);
Ja (1,5) = Ja (1,2);
Ja (1,6) = Ja (1,2);
Ja (1,7) = K(1)*F(1)*F7x/Ft^2;

Ja (2,1) = -0.848*K(2)*F(2)/Ft^2 + 0.047*K(1)*(Ft + 0.848*F(1))/Ft^2;
Ja (2,2) = - 1/V + (-K(2)*(Ft-F(2)) - 0.047*K(1)*F(1))/Ft^2;
Ja (2,3) = (K(2)*F(2) - 0.047*K(1)*F(1))/Ft^2;
Ja (2,4) = Ja (2,3);
Ja (2,5) = Ja (2,3);
Ja (2,6) = Ja (2,3);
Ja (2,7) = F7x*(K(2)*F(2) - 0.047*K(1)*F(1))/Ft^2;

Ja (3,1) = - 0.848*(4*K(3)*F(3)^2 + 2*K(4)*F(3)*F(4))/Ft^3;
Ja (3,2) = (4*K(3)*F(3)^2 + 2*K(4)*F(3)*F(4))/Ft^3;
Ja (3,5) = Ja (3,2);
Ja (3,6) = Ja (3,2);
Ja (3,3) = - 1/V -(4*K(3)*F(3)*Ft - 4*K(3)*F(3)^2 +K(4)*F(4)*Ft-2*K(4) ...
             *F(3)*F(4))/Ft^3;
Ja (3,4) = (4*K(3)*F(3)^2 - K(4)*F(3)*Ft + 2*K(4)*F(3)*F(4))/Ft^3;
Ja (3,7) = F7x*(4*K(3)*F(3)^2 + 2*K(4)*F(3)*F(4))/Ft^3;

Ja (4,1) = -0.848*2*K(4)*F(3)*F(4)/Ft^3+0.073*K(1)*(Ft + 0.848*F(1))/Ft^2;
Ja (4,2) = 2*K(4)*F(3)*F(4)/Ft^3 - 0.073*K(1)*F(1)/Ft^2;
Ja (4,5) = Ja (4,2);
Ja (4,6) = Ja (4,2);
Ja (4,3) = -(K(4)*F(4)*Ft - 2*K(4)*F(3)*F(4))/Ft^3 - 0.073*K(1)*F(1)/Ft^2;
Ja (4,4) = - 1/V -(K(4)*F(3)*Ft - 2*K(4)*F(3)*F(4))/Ft^3 - 0.073*K(1) ...
             *F(1)/Ft^2;
Ja (4,7) = F7x*(2*K(4)*F(3)*F(4)/Ft^3 - 0.073*K(1)*F(1)/Ft^2);
```

```
Ja (5,1) = - 0.848*2*K(3)*F(3)^2/Ft^3;
Ja (5,2) = 2*K(3)*F(3)^2/Ft^3;
Ja (5,4) = Ja (5,2);
Ja (5,6) = Ja (5,2);
Ja (5,3) = -2*K(3)*(F(3)*Ft - F(3)^2)/Ft^3;
Ja (5,5) = 1/V + 2*K(3)*F(3)^2/Ft^3;
Ja (5,7) = F7x*2*K(3)*F(3)^2/Ft^3;

Ja (6,1) = - 0.848*2*K(4)*F(3)*F(4)/Ft^3;
Ja (6,2) = 2*K(4)*F(3)*F(4)/Ft^3;
Ja (6,5) = Ja (6,2);
Ja (6,6) = 1/V + 2*K(4)*F(3)*F(4)/Ft^3;
Ja (6,3) = - (K(4)*F(4)*Ft - 2*K(4)*F(3)*F(4))/Ft^3;
Ja (6,4) = - (K(4)*F(3)*Ft - 2*K(4)*F(3)*F(4))/Ft^3;
Ja (6,7) = F7x*2*K(4)*F(3)*F(4)/Ft^3 ;

Ja (7,1) = - 0.848*0.206*K(2)*F(2)/Ft^2;
Ja (7,2) = - 0.206*K(2)*(Ft - F(2))/Ft^2;
Ja (7,3) = 0.206*K(2)*F(2)/Ft^2;
Ja (7,4) = Ja (7,3);
Ja (7,5) = Ja (7,3);
Ja (7,6) = Ja (7,3);
Ja (7,7) = 1/V + F7x*0.206*K(2)*F(2)/Ft^2;



% ------------------------------------------------------------------------

% Newton Method

function [X,conv, count] = Newton_CSTR (Fun,Jac,X,Xo,K,V,tol,displ)

if nargin < 7
    tol = epsi
    displ = Oi
end
conv = 1;
n = length(X);
max = 50;
count = 0;
f = 1;
while (norm (f) > tol) & (count < max)
    f = feval (Fun,X,Xo,K,V); %Fun_CSTR(F,Fo,K,V)
    J = feval (Jac,X,Xo,K,V); %Jac_CSTR(F,Fo,K,V)
    X = X - J\f;
    count = count + 1;
    if (norm(f) > 1e16)
        conv = 0;
       break;
    end

    if displ == 1
      fprintf(1,'Iter.#=%3i Normal=%3i
Resid=%12.5e\n',count,norm(X),norm(f))
    end
end %while
if (count >= max) I (norm(f) > 1e20)
    fprintf(1, 'Newton fails at a parameter value of %12.2e\n',param)
    conv = 0;
end
```

APPENDIX B
IMPLICATIONS OF THE RESIDENCE TIME DISTRIBUTION

A simulation was run for evaluating the sensitivity of the boundary for aerosol formation with respect to the RTD. We may recall from Section 4.3 that the fluid coker RTD is in between the PFR and the one for the CSTR. Figure B.1 illustrates the locus for the two continuous flow reactors, for the same set of conditions. We can notice that the boundary for aerosol formation does not change significantly for the two different reactors. The conversion levels for the PFR where slightly higher than those for the CSTR as expected; being more significant for 1,3-butadiene, where for the case in which tetralin composition is zero was 17.4 % for the PFR and 15.4 % for the CSTR (See detailed data in tables E.1 and E.11).

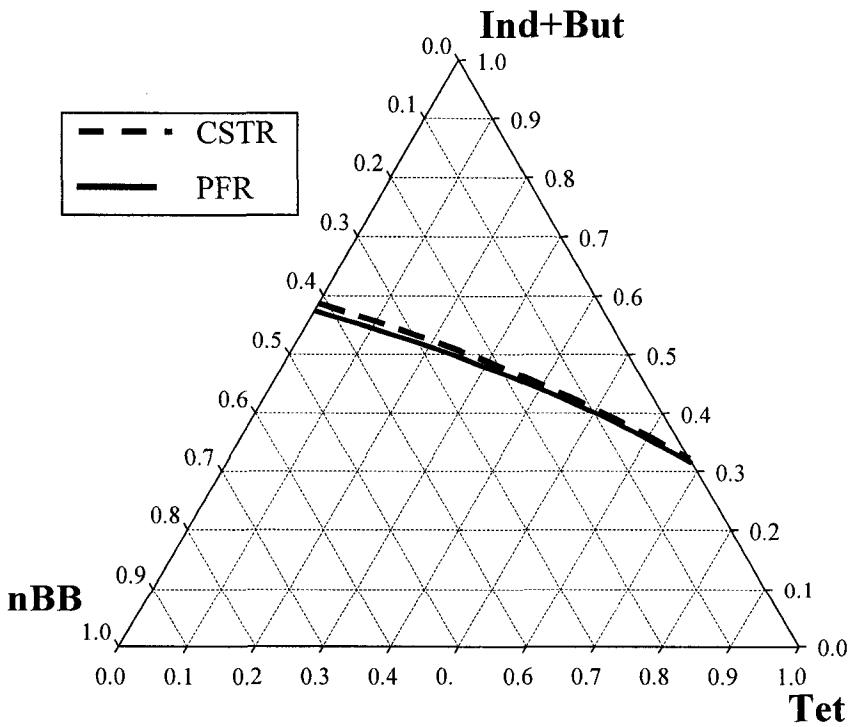

Figure B.1. Implications of the RTD
Reaction temperature 530 °C, total pressure 265 kPa, 11.5 s, wet, and O/DO of 9

Since, the actual levels of conversion are somewhere in between the two types of reactors and the boundary for aerosol formation does not change significantly any reactor chosen will give reasonable results. However, in order to favour the formation of aerosols (i.e. conservative simulation) the PFR was selected for the simulations.

APPENDIX C
LINEAR REGRESSION OF N-BUTYLBENZENE CRACKING PRODUCT DISTRIBUTION

Table C.1. Linear regression for styrene

Regression Statistics	
Multiple R	0.9998
R Square	0.9996
Std. Error	0.0818
Observations	3.0000

ANOVA

	df	*SS*	*MS*	*F*	*Sign. F*
Regression	1.0000	37.7846	37.7846	5652	0.0085
Residual	2.0000	0.0134	0.0067		
Total	3.0000	37.7979			

	Coefficients	*Std Error*	*t Stat*	*P-value*	*Lower 95%*	*Upper 95%*
Intercept	0.0000	#N/A	#N/A	#N/A	#N/A	#N/A
X Variable 1	0.6934	0.0056	124.4440	0.0001	0.6694	0.7174

Table C.2. Linear regression for ethylene

Regression Statistics	
Multiple R	0.9972
R Square	0.9944
Std. Error	0.2934
Observations	3.0000

ANOVA

	df	*SS*	*MS*	*F*	*Sign. F*
Regression	1.0000	30.6956	30.6956	356.4	0.0337
Residual	2.0000	0.1722	0.0861		
Total	3.0000	30.8678			

	Coefficients	*Std. Error*	*t Stat*	*P-value*	*Lower 95%*	*Upper 95%*
Intercept	0.0000	#N/A	#N/A	#N/A	#N/A	#N/A
X Variable 1	0.6172	0.0200	30.8608	0.0010	0.5311	0.7032

Table C.3. Linear regression for toluene

Regression Statistics	
Multiple R	1.0000
R Square	1.0000
Std. Error	0.0047
Observations	3.0000

ANOVA

	df	*SS*	*MS*	*F*	*Sign. F*
Regression	1.0000	2.5396	2.5396	114130	0.0019
Residual	2.0000	0.0000	0.0000		
Total	3.0000	2.5396			

	Coefficients	*Std. Error*	*t Stat*	*P-value*	*Lower 95%*	*Upper 95%*
Intercept	0.0000	#N/A	#N/A	#N/A	#N/A	#N/A
X Variable 1	0.1807	0.0003	562.0546	0.0000	0.1793	0.1821

Table C.4. Linear regression for propylene

Regression Statistics	
Multiple R	0.9996
R Square	0.9993
Std. Error	0.0346
Observations	3.0000

ANOVA

	df	*SS*	*MS*	*F*	*Sign. F*
Regression	1.0000	3.3307	3.3307	2785	0.0121
Residual	2.0000	0.0024	0.0012		
Total	3.0000	3.3331			

	Coefficients	*Std. Error*	*t Stat*	*P-value*	*Lower 95%*	*Upper 95%*
Intercept	0.0000	#N/A	#N/A	#N/A	#N/A	#N/A
X Variable 1	0.2055	0.0024	87.2012	0.0001	0.1954	0.2156

Table C.5. Linear regression for ethylbenzene

Regression Statistics	
Multiple R	0.9840
R Square	0.9683
Std. Error	0.0391
Observations	3.0000

ANOVA

	df	*SS*	*MS*	*F*	*Sign. F*
Regression	1.0000	0.0931	0.0931	60.9983	0.0811
Residual	2.0000	0.0031	0.0015		
Total	3.0000	0.0962			

	Coefficients	*Std. Error*	*t Stat*	*P-value*	*Lower 95%*	*Upper 95%*
Intercept	0.0000	#N/A	#N/A	#N/A	#N/A	#N/A
X Variable 1	0.0332	0.0027	12.4704	0.0064	0.0218	0.0447

Table C.6. Linear regression for ethene

Regression Statistics	
Multiple R	0.9319
R Square	0.8685
Std. Error	0.3031
Observations	3.0000

ANOVA

	df	*SS*	*MS*	*F*	*Sign. F*
Regression	1.0000	1.2141	1.2141	13.2120	0.1709
Residual	2.0000	0.1838	0.0919		
Total	3.0000	1.3978			

	Coefficients	*Std. Error*	*t Stat*	*P-value*	*Lower 95%*	*Upper 95%*
Intercept	0.0000	#N/A	#N/A	#N/A	#N/A	#N/A
X Variable 1	0.1365	0.0207	6.6057	0.0222	0.0476	0.2254

Table C.7. Linear regression for allylbenzene

Regression Statistics	
Multiple R	0.9959
R Square	0.9918
Std. Error	0.0314
Observations	3.0000

ANOVA

	df	*SS*	*MS*	*F*	*Sign. F*
Regression	1.0000	0.2388	0.2388	241.7	0.0409
Residual	2.0000	0.0020	0.0010		
Total	3.0000	0.2408			

	Coefficients	*Std. Error*	*t Stat*	*P-value*	*Lower 95%*	*Upper 95%*
Intercept	0.0000	#N/A	#N/A	#N/A	#N/A	#N/A
X Variable 1	0.0565	0.0021	26.3789	0.0014	0.0473	0.0657

Table C.8. Linear regression for methane

Regression Statistics	
Multiple R	0.9869
R Square	0.9740
Std. Error	0.0923
Observations	3.0000

ANOVA

	df	*SS*	*MS*	*F*	*Sign. F*
Regression	1.0000	0.6378	0.6378	74.83	0.0733
Residual	2.0000	0.0170	0.0085		
Total	3.0000	0.6549			

	Coefficients	*Std. Error*	*t Stat*	*P-value*	*Lower 95%*	*Upper 95%*
Intercept	0.0000	#N/A	#N/A	#N/A	#N/A	#N/A
X Variable 1	0.0939	0.0063	14.9217	0.0045	0.0668	0.1210

Table C.9. Linear regression for benzene

Regression Statistics	
Multiple R	0.9395
R Square	0.8826
Std. Error	0.0202
Observations	3.0000

ANOVA

	df	*SS*	*MS*	*F*	*Sign. F*
Regression	1.0000	0.0062	0.0062	15.03	0.1607
Residual	2.0000	0.0008	0.0004		
Total	3.0000	0.0070			

	Coefficients	*Std. Error*	*t Stat*	*P-value*	*Lower 95%*	*Upper 95%*
Intercept	0.0000	#N/A	#N/A	#N/A	#N/A	#N/A
X Variable 1	0.0097	0.0014	7.0074	0.0198	0.0037	0.0156

Table C.10. Linear regression for 1,2-dibenzil ethane

Regression Statistics	
Multiple R	0.7619
R Square	0.5804
Std. Error	0.0502
Observations	3.0000

ANOVA

	df	*SS*	*MS*	*F*	*Sign. F*
Regression	1.0000	0.0070	0.0070	2.7670	0.3446
Residual	2.0000	0.0050	0.0025		
Total	3.0000	0.0120			

	Coefficients	*Std. Error*	*t Stat*	*P-value*	*Lower 95%*	*Upper 95%*
Intercept	0.0000	#N/A	#N/A	#N/A	#N/A	#N/A
X Variable 1	0.0115	0.0034	3.3708	0.0779	-0.0032	0.0263

APPENDIX D
ADDITION REACTION BETWEEN INDENE AND 1,3-BUTADIENE

Dr. Daisuke Nohara from the Department of Biomolecular Science of the Faculty of Engineering at Gifu University in Japan provided their unpublished data for the addition reaction between indene and 1,3-butadiene. The data is the results of his work with Dr. Tomoya Sakai with batch reactors. The rate constants were estimated from the initial rate of reaction $\left(\frac{d[4HF]}{dt}\right)$ and using eq. D.1. Table D.1 shows the data and the corresponding rate constant value for the temperatures specified below:

$$\frac{d[4HF]}{dt} = k[\text{Indene}][\text{Butadiene}] \qquad (D.1)$$

Table D.1. Kinetic data for the addition reaction between indene and 1,3-butadiene

Temperature, °C	370	390	410	500
Reaction rate, mol/(L.s)	2.54E-6	4.02E-6	5.16E-6	-
Concentration of indene, mol/L	9.5E-3	9.18E-3	8.58E-3	-
Concentration of butadiene, mol/L	9.5E-3	9.78E-3	9.73E-3	-
Rate constant, L/(mol.s)	0.0281	0.0448	0.0619	0.377

APPENDIX E
CRITICAL PROPERTIES AND INTERACTION PARAMETERS

Table E.1. Critical properties of the species involved

	Critical Temperature, °C	Critical Pressure, kPa	Acentric Factor
Tetralin (Tet)	447	3620	0.3277
n-Butylbenzene (nBB)	387.4	2886.81	0.3930
1,3-butadiene (But)	151.9	4326.56	0.1949
Indene (Ind)	413.9	3820	0.3352
Vinylcyclohexene (VCH)	325.9	3430	0.3294
1,4,4a,9a-Tetra hydrofluorene (4HF)	512.6	2989.32	0.4275
Propylene (C3=)	91.8	4620.41	0.1480
Naphthalene (Nap)	475.2	4050.87	0.3024
1,2-dihydro naphthalene (DHN)	444.8	3727.11	0.3468
Hydrogen (H2)	-239.7	1315.5	-0.1201
Toluene (Tol)	318.6	4100.04	0.2596
Allylbenzene (AB)	367.8	3423.86	0.3186
Benzene (Bzn)	288.9	4924.39	0.2150
Diphenylethane (DBE)	500.4	2481.61	0.5419
Styrene (Sty)	362.9	3840	0.2971
Ethane (C2)	32.3	4883.85	9.86E-02
Ethylene (C2=)	9.2	5031.79	8.50E-02
Ethylbenzene (EB)	343.9	3607.12	0.3010
Methane (C1)	-82.5	4640.68	1.15E-02
H_2O	374.1	22120	0.3440

Table E.2. Interaction parameters (k_{ij})

	Tet	nBB	But	Ind	VCH	4HF	C3=	Nap	DHN	H2	Tol	AB	Bzn	DBE	Sty	C2	C2=	EB	C1	H2O
Tet	--	4.5E-04	7.0E-03	7.6E-04	6.2E-04	8.9E-04	1.1E-02	3.6E-04	3.1E-04	0.292	1.9E-03	3.5E-04	4.2E-03	2.0E-03	1.0E-03	1.7E-02	2.1E-02	6.8E-04	3.1E-02	0.48
nBB	4.5E-04	--	9.4E-03	1.5E-03	1.3E-03	3.5E-04	1.4E-02	7.8E-04	6.2E-04	0.292	3.1E-03	7.5E-04	6.1E-03	1.0E-03	1.9E-03	2.0E-02	2.5E-02	1.4E-03	3.6E-02	0.48
But	7.0E-03	9.4E-03	--	4.0E-03	4.4E-03	1.2E-02	1.1E-03	5.7E-03	6.2E-03	0.292	2.2E-03	5.8E-03	8.5E-04	1.5E-02	3.4E-03	2.8E-03	4.6E-03	4.2E-03	9.5E-03	0.48
Ind	7.6E-04	1.5E-03	4.0E-03	--	3.5E-04	2.5E-03	7.4E-03	4.8E-04	5.9E-04	0.292	6.9E-04	5.0E-04	2.1E-03	4.3E-03	3.7E-04	1.2E-02	1.6E-02	3.4E-04	2.4E-02	0.48
VCH	6.2E-04	1.3E-03	4.4E-03	3.5E-04	--	2.1E-03	8.0E-03	4.0E-04	4.8E-04	0.292	8.2E-04	4.1E-04	2.4E-03	3.8E-03	4.2E-04	1.3E-02	1.6E-02	3.3E-04	2.5E-02	0.48
4HF	8.9E-04	3.5E-04	1.2E-02	2.5E-03	2.1E-03	--	1.7E-02	1.4E-03	1.2E-03	0.292	4.5E-03	1.4E-03	8.0E-03	4.6E-04	3.0E-03	2.4E-02	2.9E-02	2.3E-03	4.0E-02	0.48
C3=	1.1E-02	1.4E-02	1.1E-03	7.4E-03	8.0E-03	1.7E-02	--	9.6E-03	1.0E-02	-0.104	4.8E-03	9.8E-03	2.3E-03	2.2E-02	6.6E-03	-1.9E-03	2.2E-03	7.7E-03	3.3E-02	0.48
Nap	3.6E-04	7.8E-04	5.7E-03	4.8E-04	4.0E-04	1.4E-03	9.6E-03	--	3.1E-04	0.292	1.3E-03	3.0E-04	3.2E-03	2.8E-03	6.5E-04	1.5E-02	1.9E-02	4.4E-04	2.8E-02	0.48
DHN	3.1E-04	6.2E-04	6.2E-03	5.9E-04	4.8E-04	1.2E-03	1.0E-02	3.1E-04	--	0.292	1.5E-03	3.1E-04	3.7E-03	2.4E-03	8.0E-04	1.6E-02	2.0E-02	5.3E-04	2.9E-02	0.48
H2	0.292	0.292	0.292	0.292	0.292	0.292	-0.104	0.292	0.292	--	0.285	0.292	0.285	0.292	0.292	0.223	0.007	0.292	0.202	-0.300
Tol	1.9E-03	3.1E-03	2.2E-03	6.9E-04	8.2E-04	4.5E-03	4.8E-03	1.3E-03	1.5E-03	0.285	--	1.3E-03	9.5E-04	6.9E-03	5.3E-04	3.4E-02	1.0E-02	7.6E-04	6.5E-02	0.48
AB	3.5E-04	7.5E-04	5.8E-03	5.0E-04	4.1E-04	1.4E-03	9.8E-03	3.0E-04	3.1E-04	0.292	1.3E-03	--	3.3E-03	2.7E-03	6.8E-04	1.5E-02	1.9E-02	4.5E-04	2.8E-02	0.48
Bzn	4.2E-03	6.1E-03	8.5E-04	2.1E-03	2.4E-03	8.0E-03	2.3E-03	3.2E-03	3.7E-03	0.285	9.5E-04	3.3E-03	--	1.1E-02	1.7E-03	2.0E-02	1.0E-02	2.2E-03	4.0E-02	0.48
DBE	2.0E-03	1.0E-03	1.5E-02	4.3E-03	3.8E-03	4.6E-04	2.2E-02	2.8E-03	2.4E-03	0.292	6.9E-03	2.7E-03	1.1E-02	--	5.0E-03	2.9E-02	3.4E-02	4.0E-03	4.6E-02	0.48
Sty	1.0E-03	1.9E-03	3.4E-03	3.7E-04	4.2E-04	3.0E-03	6.6E-03	6.5E-04	8.0E-04	0.292	5.3E-04	6.8E-04	1.7E-03	5.0E-03	--	1.1E-02	1.4E-02	4.0E-04	2.2E-02	0.48
C2	1.7E-02	2.0E-02	2.8E-03	1.2E-02	1.3E-02	2.4E-02	-1.9E-03	1.5E-02	1.6E-02	0.223	3.4E-02	1.5E-02	2.0E-02	2.9E-02	1.1E-02	--	1.2E-02	1.2E-02	3.0E-03	0.50
C2=	2.1E-02	2.5E-02	4.6E-03	1.6E-02	1.6E-02	2.9E-02	2.2E-03	1.9E-02	2.0E-02	0.007	1.0E-02	1.9E-02	1.0E-02	3.4E-02	1.4E-02	1.2E-02	--	1.6E-02	2.2E-02	0.48
EB	6.8E-04	1.4E-03	4.2E-03	3.4E-04	3.3E-04	2.3E-03	7.7E-03	4.4E-04	5.3E-04	0.292	7.6E-04	4.5E-04	2.2E-03	4.0E-03	4.0E-04	1.2E-02	1.6E-02	--	2.5E-02	0.48
C1	3.1E-02	3.6E-02	9.5E-03	2.4E-02	2.5E-02	4.0E-02	3.3E-02	2.8E-02	2.9E-02	0.202	6.5E-02	2.8E-02	4.0E-02	4.6E-02	2.2E-02	3.0E-03	2.2E-02	2.5E-02	--	0.50
H2O	0.48	0.48	0.48	0.48	0.48	0.48	0.48	0.48	0.48	-0.300	0.48	0.48	0.48	0.48	0.48	0.50	0.48	0.48	0.50	--

APPENDIX F
SIMULATION RESULTS

Table F.1. Results at typical fluid coker conditions
(Data used in the sensitive analysis figures 5.1, 5.3, 5.7 and B.1)

Temperature (°C)	Pressure (kPa)	Reaction Time (s)	Steam	O/DO	Initial molar fraction			Conversion of the reactants[1], %				Dew Point (°C)	Type of Reactor
					Tet	nBB	Ind+But	Tet	nBB	But	Ind		
530	265	11.5	WET	9	0.000	0.417	0.583	0.0%	6.3%	17.1%	0.7%	192.3	PFR
530	265	11.5	WET	9	0.100	0.347	0.553	1.1%	6.2%	16.4%	0.7%	195.9	PFR
530	265	11.5	WET	9	0.200	0.279	0.521	1.1%	6.2%	15.6%	0.6%	199.2	PFR
530	265	11.5	WET	9	0.300	0.215	0.485	1.1%	6.2%	14.7%	0.6%	202.4	PFR
530	265	11.5	WET	9	0.400	0.153	0.447	1.1%	6.1%	13.7%	0.5%	205.4	PFR
530	265	11.5	WET	9	0.500	0.095	0.405	1.1%	6.0%	12.5%	0.4%	208.3	PFR
530	265	11.5	WET	9	0.600	0.041	0.359	1.1%	5.5%	11.3%	0.3%	211.0	PFR
530	265	11.5	WET	9	0.680	0.000	0.320	1.1%	0.0%	10.2%	0.2%	213.1	PFR

[1] Conversion = (initial moles – final moles)/initial moles

Table F.2. Results of the simulation for the longest reaction time
(Data used in Figure 5.2)

Temperature (°C)	Pressure (kPa)	Reaction Time (s)	Steam	O/DO	Initial molar fraction			Conversion of the reactants				Dew Point (°C)	Type of Reactor
					Tet	nBB	Ind+But	Tet	nBB	But	Ind		
530	265	17	WET	9	0.000	0.411	0.589	0.0%	9.1%	23.7%	1.0%	192.3	PFR
530	265	17	WET	9	0.100	0.342	0.558	1.6%	9.1%	22.8%	1.0%	195.9	PFR
530	265	17	WET	9	0.200	0.275	0.525	1.6%	9.0%	21.7%	0.9%	199.2	PFR
530	265	17	WET	9	0.300	0.211	0.489	1.6%	9.0%	20.5%	0.8%	202.4	PFR
530	265	17	WET	9	0.400	0.150	0.450	1.6%	8.9%	19.2%	0.7%	205.4	PFR
530	265	17	WET	9	0.500	0.093	0.407	1.7%	8.7%	17.7%	0.6%	208.3	PFR
530	265	17	WET	9	0.600	0.039	0.361	1.7%	8.0%	16.0%	0.5%	211.0	PFR
530	265	17	WET	9	0.677	0.000	0.323	1.7%	0.0%	14.5%	0.3%	213.1	PFR

Table F.3. Results of the simulation for the shortest reaction time
(Data used in Figure 5.2)

Temperature (°C)	Pressure (kPa)	Reaction Time (s)	Steam	O/DO	Initial molar fraction			Conversion of the reactants				Dew Point (°C)	Type of Reactor
					Tet	nBB	Ind+But	Tet	nBB	But	Ind		
530	265	6	WET	9	0.000	0.423	0.577	0.0%	3.3%	9.6%	0.4%	192.4	PFR
530	265	6	WET	9	0.100	0.352	0.548	0.6%	3.3%	9.1%	0.4%	195.9	PFR
530	265	6	WET	9	0.200	0.284	0.516	0.6%	3.3%	8.6%	0.3%	199.2	PFR
530	265	6	WET	9	0.300	0.219	0.481	0.6%	3.3%	8.1%	0.3%	202.4	PFR
530	265	6	WET	9	0.400	0.156	0.444	0.6%	3.3%	7.5%	0.3%	205.4	PFR
530	265	6	WET	9	0.500	0.098	0.402	0.6%	3.2%	6.9%	0.2%	208.3	PFR
530	265	6	WET	9	0.600	0.043	0.357	0.6%	3.0%	6.1%	0.2%	211.0	PFR
530	265	6	WET	9	0.684	0.000	0.316	0.6%	0.0%	5.5%	0.1%	213.2	PFR

Table F.4. Results of the simulation for the dry condition (no steam present)
(Data used in Figure 5.3)

Temperature (°C)	Pressure (kPa)	Reaction Time (s)	Steam	O/DO	Initial molar fraction			Conversion of the reactants				Dew Point (°C)	Type of Reactor
					Tet	nBB	Ind+But	Tet	nBB	But	Ind		
530	265	11.5	DRY	9	0.000	0.472	0.528	0.0%	6.2%	26.6%	1.2%	223.0	PFR
530	265	11.5	DRY	9	0.100	0.399	0.501	1.1%	6.2%	25.5%	1.1%	226.7	PFR
530	265	11.5	DRY	9	0.200	0.329	0.471	1.1%	6.2%	24.4%	1.0%	230.2	PFR
530	265	11.5	DRY	9	0.300	0.261	0.439	1.1%	6.2%	23.1%	1.0%	233.5	PFR
530	265	11.5	DRY	9	0.400	0.195	0.405	1.1%	6.2%	21.7%	0.9%	236.8	PFR
530	265	11.5	DRY	9	0.500	0.132	0.368	1.1%	6.1%	20.0%	0.7%	239.8	PFR
530	265	11.5	DRY	9	0.600	0.072	0.328	1.1%	5.9%	18.2%	0.6%	242.8	PFR
530	265	11.5	DRY	9	0.729	0.000	0.271	1.1%	0.0%	15.5%	0.4%	246.5	PFR

Table F.5. Results of the simulation for the highest pressure
(Data used in Figure 5.4)

Temperature (°C)	Pressure (kPa)	Reaction Time (s)	Steam	O/DO	Initial molar fraction			Conversion of the reactants				Dew Point (°C)	Type of Reactor
					Tet	nBB	Ind+But	Tet	nBB	But	Ind		
530	350	11.5	WET	9	0.000	0.444	0.556	0.0%	6.2%	20.8%	0.9%	204.4	PFR
530	350	11.5	WET	9	0.100	0.373	0.527	1.1%	6.2%	19.9%	0.8%	208.0	PFR
530	350	11.5	WET	9	0.200	0.304	0.496	1.1%	6.2%	19.0%	0.8%	211.4	PFR
530	350	11.5	WET	9	0.300	0.237	0.463	1.1%	6.2%	17.9%	0.7%	214.6	PFR
530	350	11.5	WET	9	0.400	0.173	0.427	1.1%	6.2%	16.7%	0.6%	217.7	PFR
530	350	11.5	WET	9	0.500	0.113	0.387	1.1%	6.1%	15.4%	0.5%	220.7	PFR
530	350	11.5	WET	9	0.600	0.056	0.344	1.1%	5.7%	13.9%	0.4%	223.5	PFR
530	350	11.5	WET	9	0.705	0.000	0.295	1.1%	0.0%	12.2%	0.3%	226.4	PFR

Table F.6. Results of the simulation for the lowest pressure
(Data used in Figure 5.4)

Temperature (°C)	Pressure (kPa)	Reaction Time (s)	Steam	O/DO	Initial molar fraction			Conversion of the reactants				Dew Point (°C)	Type of Reactor
					Tet	nBB	Ind+But	Tet	nBB	But	Ind		
530	100	11.5	WET	9	0.000	0.320	0.680	0.0%	6.3%	8.2%	0.3%	154.9	PFR
530	100	11.5	WET	9	0.100	0.256	0.644	1.1%	6.2%	7.8%	0.3%	158.3	PFR
530	100	11.5	WET	9	0.200	0.195	0.605	1.1%	6.2%	7.4%	0.3%	161.4	PFR
530	100	11.5	WET	9	0.300	0.138	0.562	1.1%	6.2%	6.9%	0.2%	164.4	PFR
530	100	11.5	WET	9	0.400	0.086	0.514	1.1%	6.0%	6.4%	0.2%	167.1	PFR
530	100	11.5	WET	9	0.500	0.037	0.463	1.1%	5.6%	5.8%	0.1%	169.7	PFR
530	100	11.5	WET	9	0.584	0.000	0.416	1.1%	0.0%	5.2%	0.1%	171.8	PFR

Table F.7. Results of the simulation for the highest temperature
(Data used in Figure 5.5)

Temperature (°C)	Pressure (kPa)	Reaction Time (s)	Steam	O/DO	Initial molar fraction			Conversion of the reactants				Dew Point (°C)	Type of Reactor
					Tet	nBB	Ind+But	Tet	nBB	But	Ind		
540	265	11.5	WET	9	0.000	0.379	0.621	0.0%	8.8%	20.6%	0.9%	192.2	PFR
540	265	11.5	WET	9	0.100	0.312	0.588	1.7%	8.8%	19.8%	0.8%	195.8	PFR
540	265	11.5	WET	9	0.200	0.247	0.553	1.7%	8.8%	18.8%	0.7%	199.2	PFR
540	265	11.5	WET	9	0.300	0.186	0.514	1.7%	8.7%	17.7%	0.7%	202.4	PFR
540	265	11.5	WET	9	0.400	0.128	0.472	1.7%	8.6%	16.5%	0.6%	205.4	PFR
540	265	11.5	WET	9	0.500	0.073	0.427	1.7%	8.4%	15.2%	0.5%	208.3	PFR
540	265	11.5	WET	9	0.646	0.000	0.354	1.7%	0.0%	12.9%	0.3%	212.2	PFR

Table F.8. Results of the simulation for the lowest temperature
(Data used in Figure 5.5)

Temperature (°C)	Pressure (kPa)	Reaction Time (s)	Steam	O/DO	Initial molar fraction			Conversion of the reactants				Dew Point (°C)	Type of Reactor
					Tet	nBB	Ind+But	Tet	nBB	But	Ind		
510	265	11.5	WET	9	0.000	0.495	0.505	0.0%	3.0%	11.2%	0.5%	192.7	PFR
510	265	11.5	WET	9	0.100	0.420	0.480	0.5%	3.0%	10.8%	0.5%	196.1	PFR
510	265	11.5	WET	9	0.200	0.346	0.454	0.5%	3.0%	10.2%	0.4%	199.4	PFR
510	265	11.5	WET	9	0.300	0.275	0.425	0.5%	3.0%	9.6%	0.4%	202.5	PFR
510	265	11.5	WET	9	0.400	0.207	0.393	0.5%	3.0%	9.0%	0.4%	205.5	PFR
510	265	11.5	WET	9	0.500	0.142	0.358	0.5%	2.9%	8.2%	0.3%	208.3	PFR
510	265	11.5	WET	9	0.600	0.081	0.319	0.5%	2.9%	7.4%	0.3%	211.0	PFR
510	265	11.5	WET	9	0.700	0.024	0.276	0.5%	2.4%	6.5%	0.2%	213.6	PFR
510	265	11.5	WET	9	0.745	0.000	0.255	0.5%	0.0%	6.0%	0.1%	214.8	PFR

Table F.9. Results of the simulation for the highest value of the olefin to diolefin ratio
(Data used in Figure 5.6)

Temperature (°C)	Pressure (kPa)	Reaction Time (s)	Steam	O/DO	Initial molar fraction			Conversion of the reactants				Dew Point (°C)	Type of Reactor
					Tet	nBB	Ind+But	Tet	nBB	But	Ind		
530	265	11.5	WET	14	0.000	0.349	0.651	0.0%	6.3%	15.7%	0.6%	193.1	PFR
530	265	11.5	WET	14	0.100	0.284	0.616	1.1%	6.2%	15.0%	0.5%	196.6	PFR
530	265	11.5	WET	14	0.200	0.223	0.577	1.1%	6.2%	14.2%	0.5%	199.9	PFR
530	265	11.5	WET	14	0.300	0.165	0.535	1.1%	6.2%	13.3%	0.4%	203.1	PFR
530	265	11.5	WET	14	0.400	0.110	0.490	1.1%	6.1%	12.3%	0.4%	206.0	PFR
530	265	11.5	WET	14	0.500	0.059	0.441	1.1%	5.9%	11.2%	0.3%	208.8	PFR
530	265	11.5	WET	14	0.626	0.000	0.374	1.1%	0.0%	9.6%	0.2%	212.1	PFR

Table F.10. Results of the simulation for the most conservative case
(Data used in Figure 5.7)

Temperature (°C)	Pressure (kPa)	Reaction Time (s)	Steam	O/DO	Initial molar fraction			Conversion of the reactants				Dew Point (°C)	Type of Reactor
					Tet	nBB	Ind+But	Tet	nBB	But	Ind		
510	350	6	DRY	9	0.000	0.585	0.415	0.0%	1.6%	12.0%	0.5%	237.9	PFR
510	350	6	DRY	9	0.100	0.505	0.395	0.3%	1.6%	11.5%	0.5%	241.4	PFR
510	350	6	DRY	9	0.200	0.427	0.373	0.3%	1.6%	10.9%	0.5%	244.9	PFR
510	350	6	DRY	9	0.300	0.351	0.349	0.3%	1.6%	10.3%	0.4%	248.2	PFR
510	350	6	DRY	9	0.400	0.276	0.324	0.3%	1.6%	9.6%	0.4%	251.5	PFR
510	350	6	DRY	9	0.500	0.203	0.297	0.3%	1.6%	8.9%	0.4%	254.6	PFR
510	350	6	DRY	9	0.600	0.134	0.266	0.3%	1.5%	8.0%	0.3%	257.7	PFR
510	350	6	DRY	9	0.700	0.067	0.233	0.3%	1.5%	7.1%	0.2%	260.6	PFR
510	350	6	DRY	9	0.807	0.000	0.193	0.3%	0.0%	5.9%	0.2%	263.7	PFR

Table F.11. Results of the simulation for the continuous stirring tank reactor (CSTR)
(Data used in Figure B.1)

Temperature (°C)	Pressure (kPa)	Reaction Time (s)	Steam	O/DO	Initial molar fraction			Conversion of the reactants				Dew Point (°C)	Type of Reactor
					Tet	nBB	Ind+But	Tet	nBB	But	Ind		
530	265	11.5	WET	9	0.000	0.407	0.593	0.0%	6.0%	15.2%	0.7%	192.3	CSTR
530	265	11.5	WET	9	0.100	0.338	0.562	1.1%	6.0%	14.6%	0.6%	195.9	CSTR
530	265	11.5	WET	9	0.200	0.272	0.528	1.1%	6.0%	14.0%	0.6%	199.2	CSTR
530	265	11.5	WET	9	0.300	0.208	0.492	1.1%	6.0%	13.3%	0.5%	202.4	CSTR
530	265	11.5	WET	9	0.400	0.148	0.452	1.1%	5.9%	12.4%	0.5%	205.4	CSTR
530	265	11.5	WET	9	0.500	0.091	0.409	1.1%	5.8%	11.5%	0.4%	208.3	CSTR
530	265	11.5	WET	9	0.600	0.037	0.363	1.1%	5.3%	10.4%	0.3%	211.0	CSTR
530	265	11.5	WET	9	0.674	0.000	0.326	1.1%	0.0%	9.5%	0.2%	213.0	CSTR